Cell Reports

Multipotent progenitors and hematopoietic stem cells arise independently from hemogenic endothelium in the mouse embryo

Graphical abstract

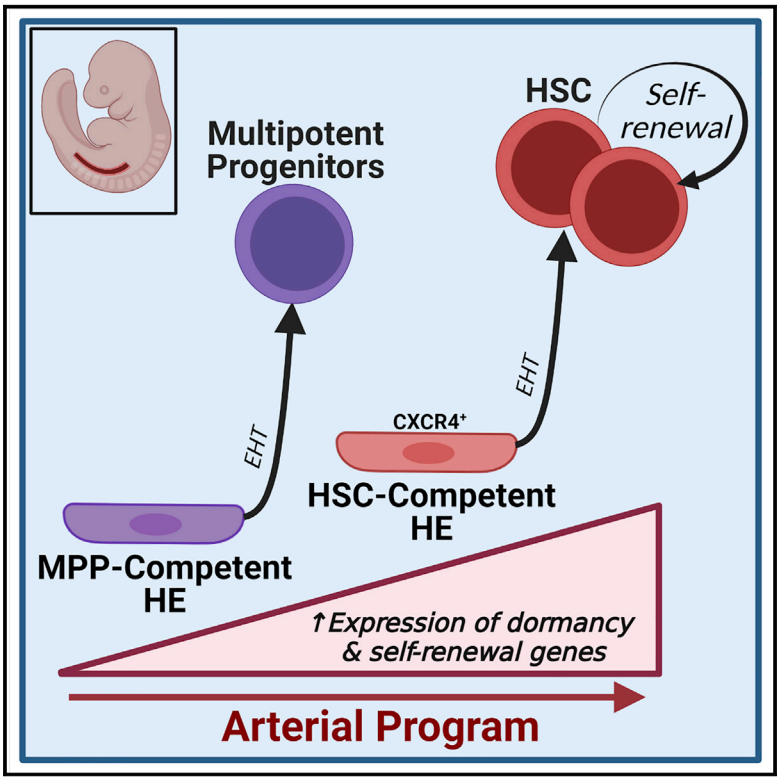

Authors

Tessa Dignum, Barbara Varnum-Finney, Sanjay R. Srivatsan, ..., Cole Trapnell, Irwin D. Bernstein, Brandon Hadland

Correspondence

bhadland@fredhutch.org

In brief

Integrating multiple single-cell approaches, Dignum et al. reveal immunophenotypic and transcriptional properties of hemogenic endothelium (HE) that are precursors to the first HSCs. They identify a population of HE with clonal multipotent hematopoietic potential distinct from HSC-competent HE and uncover arterial-associated transcriptional programs linked to HSC competence.

Highlights

- HSC-competent HE are characterized by CXCR4 surface expression
- Multipotent progenitor potential is initially uncoupled from HSC potential
- HSC-competent HE express arterial-associated dormancy and self-renewal genes

Dignum et al., 2021, Cell Reports *36*, 109675
September 14, 2021
https://doi.org/10.1016/j.celrep.2021.109675

Cell Reports

CellPress
OPEN ACCESS

Report

Multipotent progenitors and hematopoietic stem cells arise independently from hemogenic endothelium in the mouse embryo

Tessa Dignum,[1] Barbara Varnum-Finney,[1] Sanjay R. Srivatsan,[3] Stacey Dozono,[1] Olivia Waltner,[1] Adam M. Heck,[1] Takashi Ishida,[1] Cynthia Nourigat-McKay,[1] Dana L. Jackson,[3] Shahin Rafii,[4] Cole Trapnell,[3] Irwin D. Bernstein,[1,2] and Brandon Hadland[1,2,5,*]

[1]Clinical Research Division, Fred Hutchinson Cancer Research Center, Seattle, WA 98109, USA
[2]Department of Pediatrics, University of Washington School of Medicine, Seattle, WA 98105, USA
[3]Department of Genome Sciences, University of Washington School of Medicine, Seattle, WA 98105, USA
[4]Department of Genetic Medicine, Ansary Stem Cell Institute, Howard Hughes Medical Institute, Weill Cornell Medical College, New York, NY 10021, USA
[5]Lead contact
*Correspondence: bhadland@fredhutch.org
https://doi.org/10.1016/j.celrep.2021.109675

SUMMARY

During embryogenesis, waves of hematopoietic progenitors develop from hemogenic endothelium (HE) prior to the emergence of self-renewing hematopoietic stem cells (HSCs). Although previous studies have shown that yolk-sac-derived erythromyeloid progenitors and HSCs emerge from distinct populations of HE, it remains unknown whether the earliest lymphoid-competent progenitors, multipotent progenitors, and HSCs originate from common HE. In this study, we demonstrate by clonal assays and single-cell transcriptomics that rare HE with functional HSC potential in the early murine embryo are distinct from more abundant HE with multilineage hematopoietic potential that fail to generate HSCs. Specifically, HSC-competent HE are characterized by expression of CXCR4 surface marker and by higher expression of genes tied to arterial programs regulating HSC dormancy and self-renewal. Taken together, these findings suggest a revised model of developmental hematopoiesis in which the initial populations of multipotent progenitors and HSCs arise independently from HE with distinct phenotypic and transcriptional properties.

INTRODUCTION

Hematopoietic stem cells (HSCs) possess simultaneous multilineage and self-renewal capacity and are defined by their ability to reconstitute the entire hematopoietic system upon transplantation to a conditioned host. HSCs emerge during embryonic development from a specialized subset of endothelial cells (ECs) with hematopoietic potential, known as hemogenic endothelium (HE). This endothelial-to-hematopoietic transition (EHT) produces the first transplantable HSCs by murine embryonic day (E)10.5–11 within arterial vessels, including the aorta of the para-aortic splanchnopleura (P-Sp)/aorta-gonad-mesonephros (AGM) region and the vitelline and umbilical arteries (de Bruijn et al., 2000; Medvinsky and Dzierzak, 1996; Müller et al., 1994). Prior to the emergence of HSCs, however, several distinct waves of progenitors arise independently to provide functioning blood cells for the developing embryo. The first of these, referred to as the primitive and erythromyeloid progenitor (EMP) waves, emerge in the yolk sac and are primarily restricted to the production of erythroid, megakaryocytic, and myeloid progeny (Iturri et al., 2021; Palis, 2016; Soares-da-Silva et al., 2021). These waves lack significant lymphoid potential, which emerges during a third wave of hematopoiesis that produces lympho-myeloid progenitors (LMPs), multipotent progenitors (MPPs), and ultimately HSCs (Böiers et al., 2013; Hadland and Yoshimoto, 2018; Inlay et al., 2014). Since clonal MPPs are detectable prior to HSC emergence, it has been postulated that they give rise to HSCs following their acquisition of additional properties necessary for HSC function, such as self-renewal (Inlay et al., 2014). However, this remains to be formally determined, as initial MPP activity has not been clonally linked to later HSC fate, and surface markers that can prospectively distinguish HE with HSC potential from those generating various categories of multilineage progenitors have not been identified. To explore this, we employed single-cell index sorting of hemogenic precursors to co-culture with AGM-derived endothelial cells (AGM-ECs) and assays for HSCs and multilineage potential. We previously reported that this co-culture system supports the formation of multilineage-engrafting HSCs from P-Sp/AGM-derived HE isolated as early as E9 (Hadland et al., 2015, 2017, 2018). Focusing our analysis on HE clonally isolated from E9 to E10 P-Sp/AGM at the onset of EHT, we found that CXCR4 expression distinguishes HSC-competent HE from progenitor-restricted HE, including a subset with *in vitro* multilineage potential. Single-cell RNA

sequencing (scRNA-seq) demonstrated that *Cxcr4*-expressing HE are simultaneously enriched in expression of arterial-specific genes and HSC self-renewal genes controlling dormancy and cell cycle, compared to the more abundant *Cxcr4*-negative HE. Altogether, our studies suggest a model in which the earliest MPPs and HSCs emerge independently from phenotypically and transcriptionally distinct populations of HE, which has important implications for long-standing efforts to generate HSCs from pluripotent stem cells.

RESULTS

CXCR4 expression marks rare clonal HE with HSC potential in the early embryo

Using AGM-EC co-culture and transplantation assays, we previously demonstrated that long-term HSC activity within the P-Sp/AGM-derived vascular endothelial (VE)-cadherin$^+$ population between E9 and E11.5 is largely restricted to cells co-expressing EPCR and CD61 (henceforth referred to as the V$^+$E$^+$61$^+$ population) (Hadland et al., 2017, 2018, 2021). Employing our previously described method of single-cell index sorting to AGM-EC co-culture followed by analysis of HSC activity—defined by detection of cells with the VE-cadherin$^{-/low}$CD45$^+$Gr1$^-$F4/80$^-$Sca1^{hi}EPCR^{hi} immunophenotype, a reliable surrogate for multilineage engraftment potential in this assay (Hadland et al., 2017, 2018)—we determined that most clonal V$^+$E$^+$61$^+$ hemogenic precursors (defined here as colony-forming cells [CFCs]) isolated between E9 and E10 generated colonies with hematopoietic progenitor cells (HPCs; HPC-CFCs) but no detectable HSCs. In contrast, clonal V$^+$E$^+$61$^+$ hemogenic precursors capable of generating HSCs (HSC-CFCs) are rare (Figures 1A and 1B). If HE with cell-intrinsic HSC potential constitute a distinct population from HE that lack HSC potential, we hypothesized that they may be prospectively isolated based on expression of unique surface markers. Previous studies have shown that arterial markers DLL4 and CD44 are expressed by HE in the P-Sp/AGM, but they do not necessarily distinguish HE with HSC potential from those restricted to progenitor fates at this early stage (Hadland et al., 2017; Oatley et al., 2020). We hypothesized that another arterial marker, CXCR4, may better predict HSC potential given our recent observation that its canonical ligand, CXCL12, is required for the generation of HSCs (but not progenitors) from P-Sp/AGM-derived hemogenic precursors in a stroma-free engineered niche (Hadland et al., 2021), and that CXCR4 is heterogeneously expressed within the V$^+$E$^+$61$^+$ population of the E9.5 P-Sp/AGM, which is enriched in arterial markers DLL4 and CD44 (Figure 1C).

To investigate whether expression of CXCR4 distinguishes clonal HSC precursors, we isolated V$^+$E$^+$61$^+$ cells from E9-E10 P-Sp/AGM for single-cell index sorting to AGM-EC co-culture (Figure 1A). This methodology allows for the retrospective correlation of the clonal hematopoietic progeny of single cells with their initial immunophenotype captured at the time of index sorting, including additional markers analyzed but not used in the sorting strategy. Correlating phenotypic HSC output following co-culture with the initial index phenotype of each V$^+$E$^+$61$^+$ starting cell, we show that the rare hemogenic precursors (including CD41$^-$CD43$^-$CD45$^-$ HE) with HSC potential (HSC-CFCs) typically express CXCR4, whereas most HPC-CFCs lack CXCR4 expression (Figures 1D, 1F, and 1G; Figures S1A and S1B). Based on our previous studies of clonal HSC precursors at this early stage, HSC-CFCs as defined by immunophenotype can be heterogeneous with regard to long-term multilineage engraftment *in vivo* (Hadland et al., 2017). Thus, to validate that clonal CXCR4$^+$ HSC-CFCs generated functional long-term HSCs, we assessed a subset of the HSC-by-phenotype colonies through transplant and confirmed their multilineage engraftment potential *in vivo* (Figure 1E; Table S1A). In addition, when we sorted the CXCR4$^+$ and CXCR4$^-$ fractions of the E9–9.5 P-Sp/AGM-derived V$^+$E$^+$ population in bulk for AGM-EC co-culture and subsequent transplantation (Figures S1C and S1D), we confirmed that HSC potential was confined to the CXCR4$^+$ subset, whereas the CXCR4$^-$ fraction generated phenotypic HPCs that lacked significant multilineage engraftment (Figure 1H; Figure S1E; Table S1B). Altogether, these findings show that CXCR4 expression marks rare HSC-competent HE in the early embryo.

Clonal HE harboring multilineage hematopoietic activity emerge independently from HSC-competent HE in the early embryo

Although most E9–10 P-Sp/AGM-derived V$^+$E$^+$61$^+$ HE generate HPCs lacking multilineage engraftment potential, the lineage potentials of clonal HPC-CFCs within this population remain undefined. In accordance with recent literature, we hypothesized that HPC-CFCs detected in our co-culture system are precursors to the initial wave of LMPs that are proposed to be HSC-independent (Böiers et al., 2013; Zhu et al., 2020). Clonal precursors with *in vitro* multilineage hematopoietic potential have also been identified in the E9–10 yolk sac and P-Sp/AGM (Inlay et al., 2014), and they were postulated to represent HSC precursors that acquire definitive HSC fate upon further maturation (thus equivalent to HSC-CFCs in our assays).

To investigate this, we explored the *in vitro* lineage potentials of clonal E9–10 HPC-CFCs following AGM-EC co-culture by secondary colony-forming unit (CFU) assays (to screen for erythroid and myeloid potential) and co-culture with OP9 or OP9-DLL4 stromal cells (to assess B- and T-lymphoid potential, respectively) (Figure 2A). Notably, we observed a variety of lineage-restricted potentials beyond LMPs, including erythromyeloid and myeloid-only, from HPC-CFCs expressing hematopoietic markers CD41, CD43, and/or CD45, as well as from HPC-CFCs with a HE phenotype (CD41$^-$CD43$^-$CD45$^-$) and HPC-CFCs expressing arterial marker CD44 (Oatley et al., 2020; Figures 2B–2D; Figures S2A and S2B). We also detected HPC-CFCs with multipotent hematopoietic potential (MPP-CFCs) that are mostly CXCR4$^-$, are more abundant than HSC-CFCs, and fail to generate phenotypic or functionally engrafting HSCs following AGM-EC culture (Figures 2B–2D; Figures S2A and S2B; and data not shown). These data demonstrate the unexpected existence of a unique population of MPP-competent HE that lack cell-intrinsic properties necessary for HSC fate.

scRNA-seq identifies the transcriptional signature of *Cxcr4*-expressing HSC-competent HE

Based on our finding that CXCR4 expression identifies rare clonal HSC-competent HE in the V$^+$E$^+$61$^+$ population, we leveraged single-cell transcriptomics to investigate the transcriptional

CellPress
OPEN ACCESS

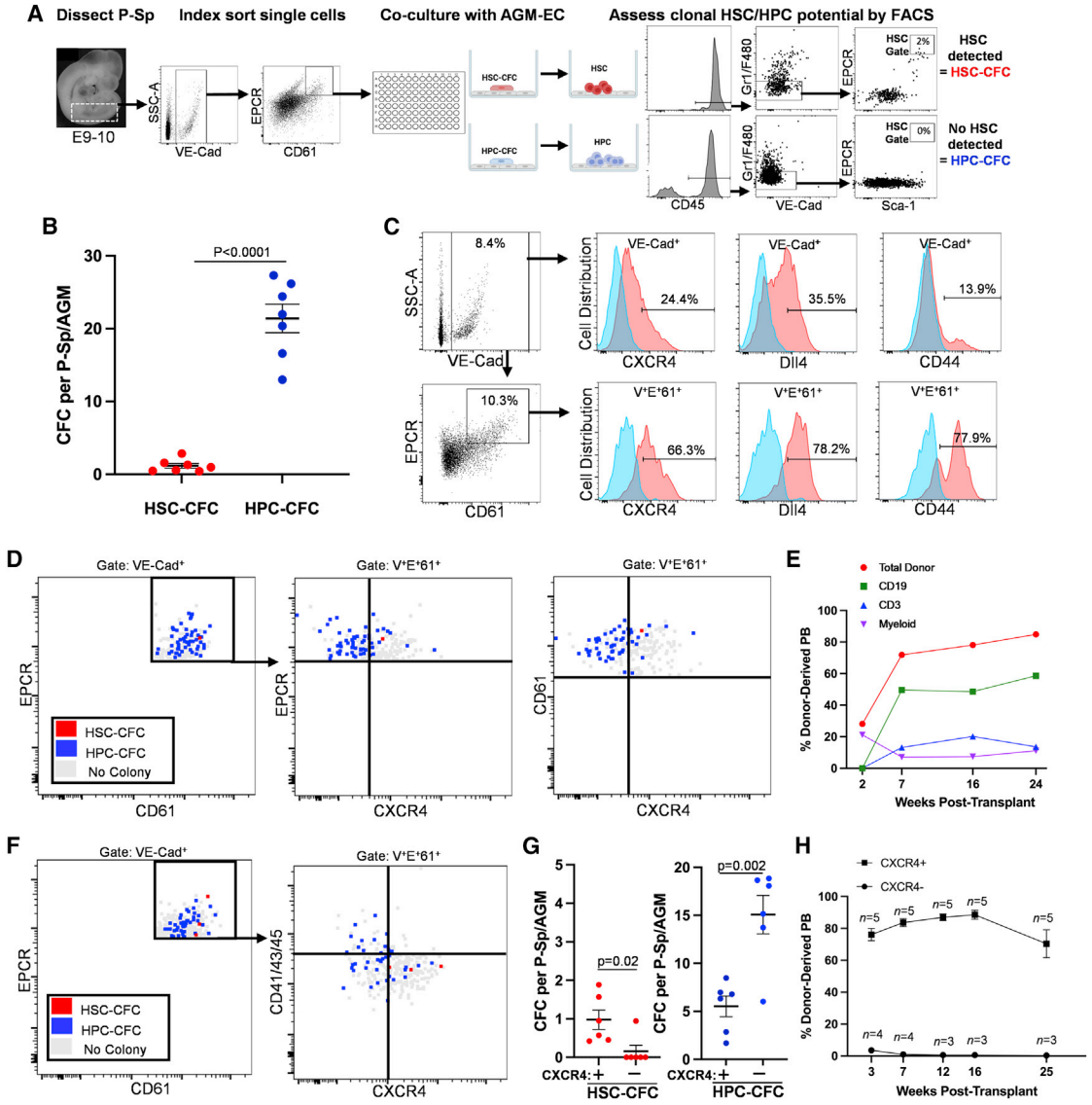

Figure 1. CXCR4 expression marks rare clonal HE with HSC potential in the early murine embryo

(A) Methodology for index sorting of single P-Sp-derived $V^+E^+61^+$ cells to co-culture on AGM-ECs and subsequent analysis to assess HSC potential. HSC colony-forming cells (HSC-CFCs) indicate clonal $V^+E^+61^+$ cells that generate colonies containing HSCs detectable by immunophenotype (VE-cadherin$^{-/low}$ CD45$^+$Gr1$^-$F4/80$^-$Sca1^{hi}EPCR^{hi}, indicated in "HSC gate"), whereas HPC-CFCs lack immunophenotypically detectable HSCs (i.e., no cells detected in the HSC gate).

(B) Number of HSC-CFCs and HPC-CFCs detected across seven independent experiments from E9 to E10 (19–30 somite pairs [sp]). Error bars show mean ± SEM. p values indicate unpaired Student's t test.

(C) Expression of CXCR4, CD44, and DLL4 in the VE-cadherin$^+$ population and the $V^+E^+61^+$ subset of E9.5 (29 sp) P-Sp. Blue histograms indicate isotype controls.

(D) Correlation of clonal HSC-CFC and HPC-CFC potential with expression of CXCR4 on individual index-sorted $V^+E^+61^+$ cells at E9.5 (26–29 sp).

(E) Donor-derived peripheral blood (PB) engraftment of clonal progeny of the single HSC-CFCs in (D), including B lymphoid (CD19), T lymphoid (CD3), and myeloid contribution.

(F) Correlation of clonal HSC-CFCs and HPC-CFCs with surface expression of CXCR4 and CD41, CD43, and CD45 on individual index-sorted $V^+E^+61^+$ cells at E9.5 (29–30 sp).

(G) Distribution of CXCR4$^+$ and CXCR4$^-$ HSC-CFCs and HPC-CFCs detected across six independent experiments from E9 to E10 (19–30 sp). Error bars show mean ± SEM. p values indicate unpaired Student's t test.

(H) Donor-derived PB engraftment of the hematopoietic progeny of bulk-sorted CXCR4$^+$ and CXCR4$^-$ cells within the V^+E^+ population at E9.5 (22–29 sp) following AGM-EC co-culture and transplantation. Error bars show mean ± SEM; n indicates number of recipient mice. All recipients of CXCR4$^+$ cells had multilineage engraftment.

See also Figure S1 and Table S1.

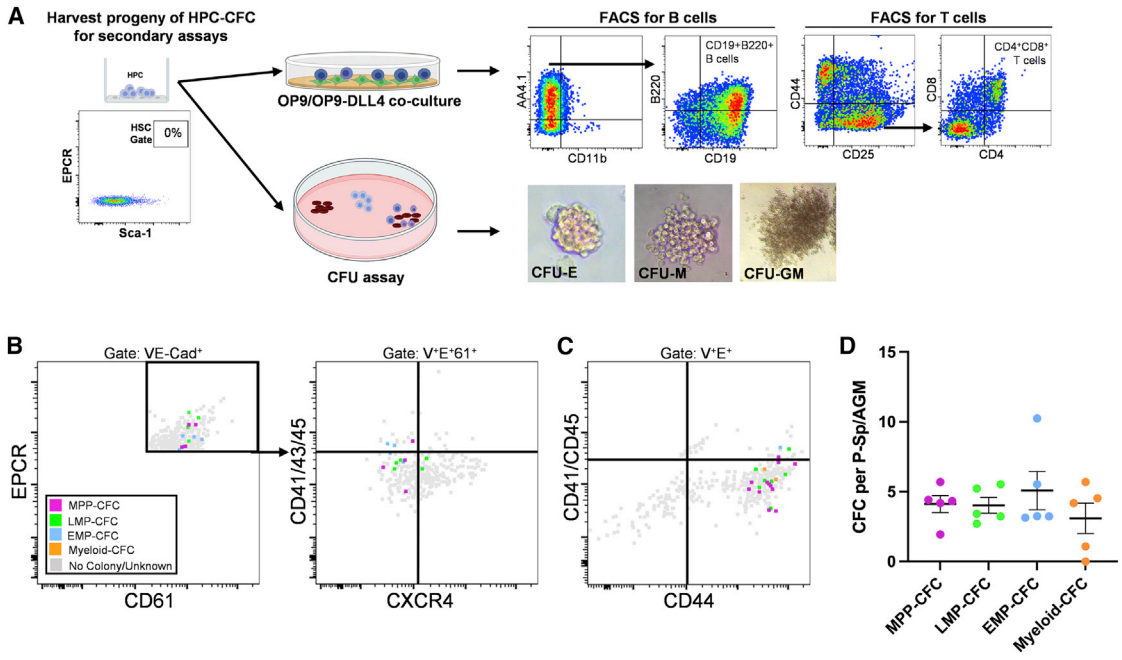

Figure 2. Clonal HE harboring multilineage hematopoietic activity emerge independently from HSC-competent HE in the early embryo

(A) Methodology for analysis of *in vitro* hematopoietic lineage potential of clonal progeny of HPC-CFCs. Representative images of erythroid colony-forming unit (CFU-E) (original magnification, ×20), macrophage CFU (CFU-M) (original magnification, ×20), and granulocyte-monocyte CFU (CFU-GM) (original magnification, ×4) shown.

(B and C) Correlation of clonal hematopoietic lineage potential with CXCR4, CD41, CD43, CD44, and CD45 expression of individual HPC-CFCs from E9.5 P-Sp (26–28 sp). Multipotent (MPP-CFCs), lymphomyeloid (LMP-CFCs), erythromyeloid (EMP-CFCs), and myeloid colony-forming cells (myeloid-CFCs). No colony/unknown (gray) indicates absence of detectable hematopoietic output following AGM-EC or secondary CFU/OP9 assays.

(D) Total progenitor CFCs within the $V^+E^+61^+$ population per P-Sp detected across five independent experiments from E9 to E10 (19–30 sp). Error bars show mean ± SEM. p values indicate unpaired Student's t test.

See also Figure S2.

landscape of hemogenic precursors differentially expressing *Cxcr4*, hypothesizing that *Cxcr4* expression would reveal the unique transcriptional state of HE with HSC potential. To this end, we dissected P-Sp from E9–9.5 embryos and sorted $V^+E^+61^+$ cells for scRNA-seq (Figures S3A and S3B). Using the Monocle3 analysis toolkit (Cao et al., 2019), we performed dimensionality reduction by uniform manifold approximation and projection (UMAP) and unsupervised clustering of the single-cell transcriptomes (Figure 3A; Figures S3C and S3D). After removing clusters expressing somite-specific genes (presumed to represent a population of contaminating cells detected in the post-sort analysis, Figures S3A and S3E), cells in the remaining clusters expressed EC marker *Cdh5* (VE-cadherin) and were heterogeneous for genes associated with arterial ECs and HE (Figure 3B), consistent with immunophenotypic and functional analysis of $V^+E^+61^+$ cells (Figures 1 and 2). A small cluster (n = 23) expressing markers of mature HPCs (e.g., *Ptprc*/CD45, *Flt3*) was also identified (Figure 3B; Figure S3F). To identify clusters associated with *Cxcr4* expression, we classified the clusters in UMAP space based on threshold detection of *Cxcr4* transcript in single cells in each cluster (Figure 3C). We then classified cells according to type on the basis of known marker genes using Garnett (Pliner et al., 2019), assigning cells as unspecified ECs, early and mature arterial ECs, HE, and HPCs (Figure 3D). Cxcr4-negative clusters were enriched in unspecified ECs, early arterial ECs, and HPCs, whereas Cxcr4-positive clusters were enriched in mature arterial ECs (Figure 3D). Both clusters contained HE, with fewer in the Cxcr4-positive clusters relative to the Cxcr4-negative clusters (Figure 3D), which is consistent with the relative frequencies of clonal CFCs between $CXCR4^+$ and $CXCR4^-$ subsets of the $V^+61^+E^+$ population in our single-cell index assays (Figures 1D and 1F; Figures S1A and S1B). We next examined the relative aggregate expression (gene-set score) of published arterial EC-specific genes (Aranguren et al., 2013; Luo et al., 2021; Xu et al., 2018). As expected, these gene-set scores were highest in cells transcriptionally classified as mature arterial ECs. Furthermore, Cxcr4-positive HE had significantly higher arterial EC gene-set scores than did Cxcr4-negative HE (Figure 3E; Figure S3G). We also examined previously published HSC-specific signature gene sets from E11 AGM (Vink et al., 2020) and adult bone marrow (Cabezas-Wallscheid et al., 2017; Chambers et al., 2007; Rodriguez-Fraticelli et al., 2020; Wilson et al., 2015). Remarkably, we found that these gene-set scores followed a similar pattern to those of arterial EC-specific genes (peaking in mature arterial ECs), and they were significantly higher in Cxcr4-positive HE than in Cxcr4-negative HE (Figure 3E; Figure S3G). When we examined expression of genes recently reported as specific to HSC-primed HE in the P-Sp/AGM

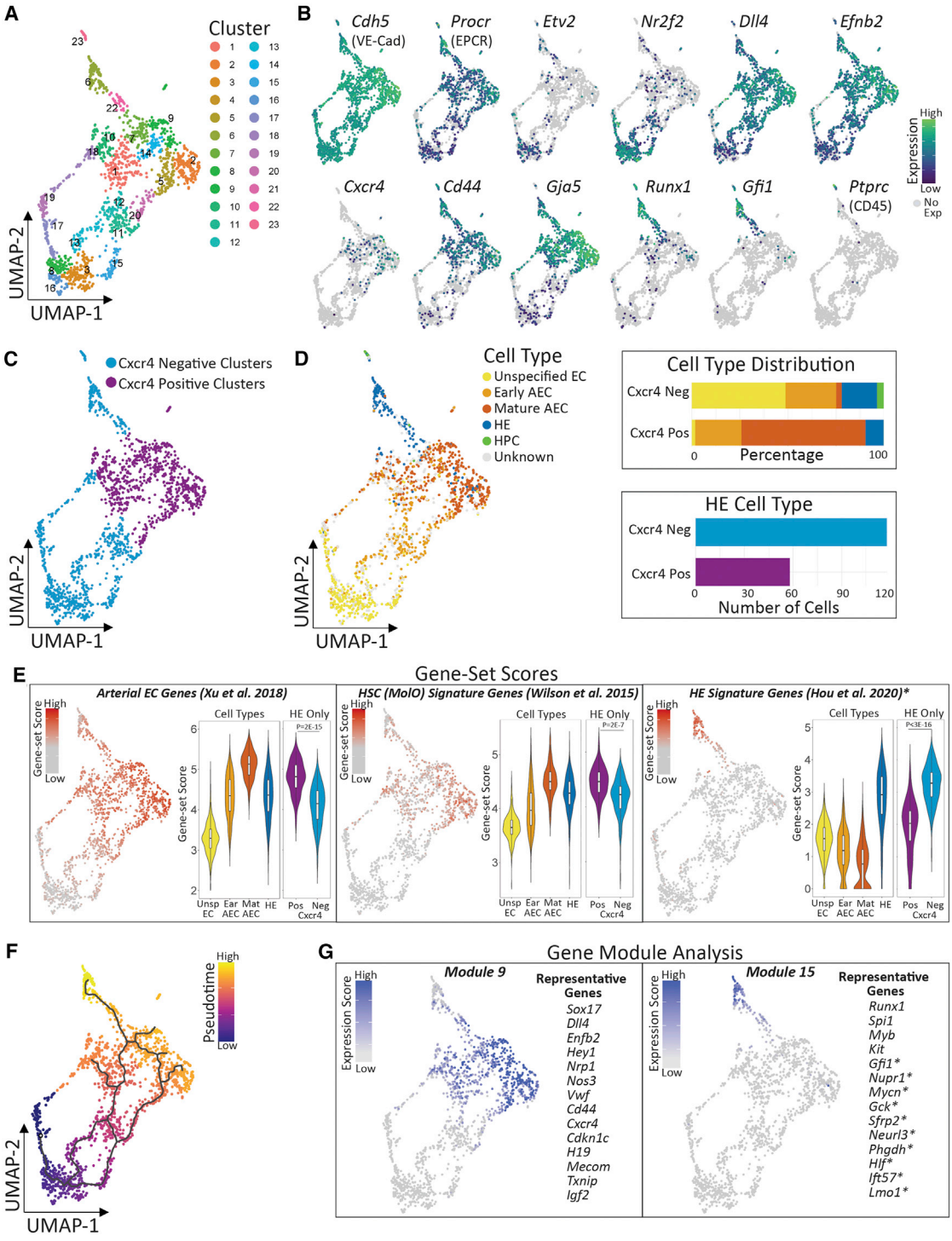

Figure 3. Single-cell RNA sequencing (scRNA-seq) identifies the transcriptional signature of *Cxcr4*-expressing HSC-competent HE

(A) UMAP and cluster analysis of scRNA-seq data from E9–9.5 P-Sp-derived $V^{+}E^{+}61^{+}$ cells (see also Figures S3A–S3D; see STAR Methods for details).

(B) Gene expression heatmap for pan-endothelial marker VE-cadherin (*Cdh5*), EPCR (*Procr*), *Cxcr4*, and selected transcripts used for cell type classification in (D).

(C) Classification of clusters based on *Cxcr4* transcript detected in >5% of cells in each cluster from (A).

(D) (Left) Cell type classification by Garnett based on marker genes (see STAR Methods for marker genes). (Right) Distribution of cell types among Cxcr4-positive and Cxcr4-negative clusters and quantification of HE cell type within Cxcr4-positive and Cxcr4-negative clusters.

(E) (Left) Heatmap of gene-set scores for signature gene sets defining arterial ECs (Xu et al., 2018), HSCs (Wilson et al., 2015), and HE (Hou et al., 2020). (Right) Violin plots of gene-set scores by cell type, and by Cxcr4-positive versus Cxcr4-negative HE. p values indicate Wilcoxon rank-sum test.

(legend continued on next page)

(Hou et al., 2020), this gene-set score peaked in the HE cell type in our data, as expected. However, it was significantly higher in Cxcr4-negative compared with Cxcr4-positive HE, suggesting that this gene set is not necessarily specific to HE with HSC competence at this early stage, but it is also expressed by HE restricted to multilineage progenitor fates (Figure 3E).

As a complementary approach to identify genes enriched in the Cxcr4-positive clusters in our scRNA-seq data, we next determined modules of genes that vary as a function of pseudotime (Cao et al., 2019; Trapnell et al., 2014; Figure 3F). This analysis revealed two unique gene modules (9 and 15) whose expression patterns correlate with regions of UMAP containing Cxcr4-positive and Cxcr4-negative HE, respectively (Figure 3G; Figure S3H). Significantly upregulated genes in module 9 include *Cxcr4*, along with arterial EC-specific genes and several genes required for HSC self-renewal (including *H19*, *Mecom*, *Cdkn1c*, *Igf2*, and *Txnip*) (Jeong et al., 2009; Kataoka et al., 2011; Matsumoto et al., 2011; Thomas et al., 2016; Venkatraman et al., 2013; Figure 3G, left panel; Table S2). In contrast, module 15 is enriched in genes associated with EHT and definitive hematopoiesis, including, notably, 10 of the 11 HE-specific signature genes identified by Hou et al. (2020) (Figure 3G, right panel; Table S2).

Finally, we applied regression analysis to identify genes that are differentially expressed between Cxcr4-positive and Cxcr4-negative HE (adjusted $p < 0.05$, Table S4). Gene Ontology analysis identified enrichment of genes in Cxcr4-positive HE associated with angiogenesis, cell motility, and adhesion, whereas Cxr4-negative HE were enriched in genes associated with protein synthesis, metabolic activity, and proliferation (Figures S4A and S4B; Table S4). Remarkably, genes enriched in Cxcr4-positive HE showed substantial overlap with published E11 AGM HSC signature genes (Vink et al., 2020) and adult HSC signature genes, particularly those identified as specific to dormant HSCs (Cabezas-Wallscheid et al., 2017), compared with Cxcr4-negative HE (Figures S4C and S4D). Furthermore, among the genes specifically enriched in Cxcr4-positive HE were many with established roles in HSC dormancy and self-renewal, including *H19*, *Cdkn1c*, *Ndn* (Necdin), *Mecom*, *Cd81*, *Eng* (Endoglin), and *Igf2* (Asai et al., 2012; Borges et al., 2019; Goyama et al., 2008; Kataoka et al., 2011; Lin et al., 2011; Matsumoto et al., 2011; Thomas et al., 2016; Venkatraman et al., 2013). Indeed, expression of these genes, as well as aggregated gene expression of a larger set of published HSC self-renewal/dormancy regulators, demonstrated a similar pattern to arterial EC and HSC signature gene sets, peaking in arterial ECs and Cxcr4-positive HE, and significantly decreasing in Cxcr4-negative HE (Figures 4A and 4B). Notably, expression of HSC self-renewal genes correlates closely with expression of arterial EC genes, as do AGM and adult HSC signature genes, suggesting a close link between early arterial programs and HSC-specifying programs in HSC-competent HE (Figure S4E).

Consistent with the established role of identified HSC self-renewal genes in regulating dormancy by inhibiting cell cycle entry, Cxcr4-positive HE exhibit a significantly lower proliferation index—a transcriptional measure of cell cycle activity—than do Cxcr4-negative HE (Figure 4C). Moreover, proliferative status is associated with expression of Myc pathway genes that promote cell cycle and metabolic activity (Luo et al., 2021). Cxcr4-negative HE express higher levels of Myc pathway genes that correlate with HE-specific gene expression (Hou et al., 2020; Figure 4D; Figures S4F and S4G). In contrast, Cxcr4-positive HE express lower levels of Myc genes together with higher Dll4-dependent arterial EC genes and genes associated with dormancy programs (such as embryonic diapause and senescence) (Dhimolea et al., 2021; Duy et al., 2021; Figure 4D; Figures S4F and S4G). Altogether, these studies identify the unique molecular signature of HSC-competent HE, supporting a model in which arterial endothelial-associated genes promoting transient dormancy and cell cycle inhibition function as early determinants of HSC fate by establishing self-renewal programs necessary to endow HE with HSC potential (Figure 4E).

DISCUSSION

In this study, we provide several insights into the acquisition of HSC fate during embryonic development. First, we demonstrate that clonal HE with HSC potential can be prospectively distinguished from more abundant HE that lack HSC potential by CXCR4 surface expression, suggesting that cell-intrinsic properties necessary for HSC competence are already established at the level of HE in the early P-Sp/AGM. Next, we provide evidence of clonal HE with multilineage hematopoietic progenitor activity that are distinct from HSC-competent HE, identifying an early wave of HSC-independent MPP activity and suggesting a paradigm in which the acquisition of multilineage hematopoietic potential is initially uncoupled from HSC potential in HE at this stage in development (Figure 4E). These findings have important implications for efforts to generate HSCs from pluripotent stem cells (PSCs), accounting for the observation that PSC-derived HE can clonally generate multilineage hematopoietic progenitors in the absence of HSC potential (Ditadi et al., 2015).

Finally, we used single-cell transcriptomics to gain insight into the transcriptional programs that regulate the HSC potential of HE, demonstrating that the Cxcr4-expressing subset of HE is enriched in genes required for HSC self-renewal that are closely associated with arterial transcriptional programs. Notably, we and others have recently shown that the retention of arterial endothelial transcriptional signatures is a key feature that distinguishes precursor (pre-)HSCs and the first engrafting HSCs from more differentiated hematopoietic progenitors in the later (E10.5–11.5) AGM (Hadland et al., 2021; Vink et al., 2020). Another recent study used single-cell approaches to identify a set of genes that distinguish "HSC-primed" HE from non-hemogenic arterial ECs in the P-Sp/AGM (Hou et al., 2020); however, we found that this set of genes is more highly expressed in Cxcr4-negative HE than in the Cxcr4-positive HE that possess HSC potential. Thus, these genes likely represent early markers and/or drivers of

(F) Pseudotime trajectory.
(G) Heatmaps for expression scores of gene modules that co-vary over pseudotime. Gene modules 9 and 15 are depicted with a selected subset of representative genes from each. * indicates genes from HE signature genes defined by Hou et al. (2020)
See also Figure S3 and Tables S2 and S3.

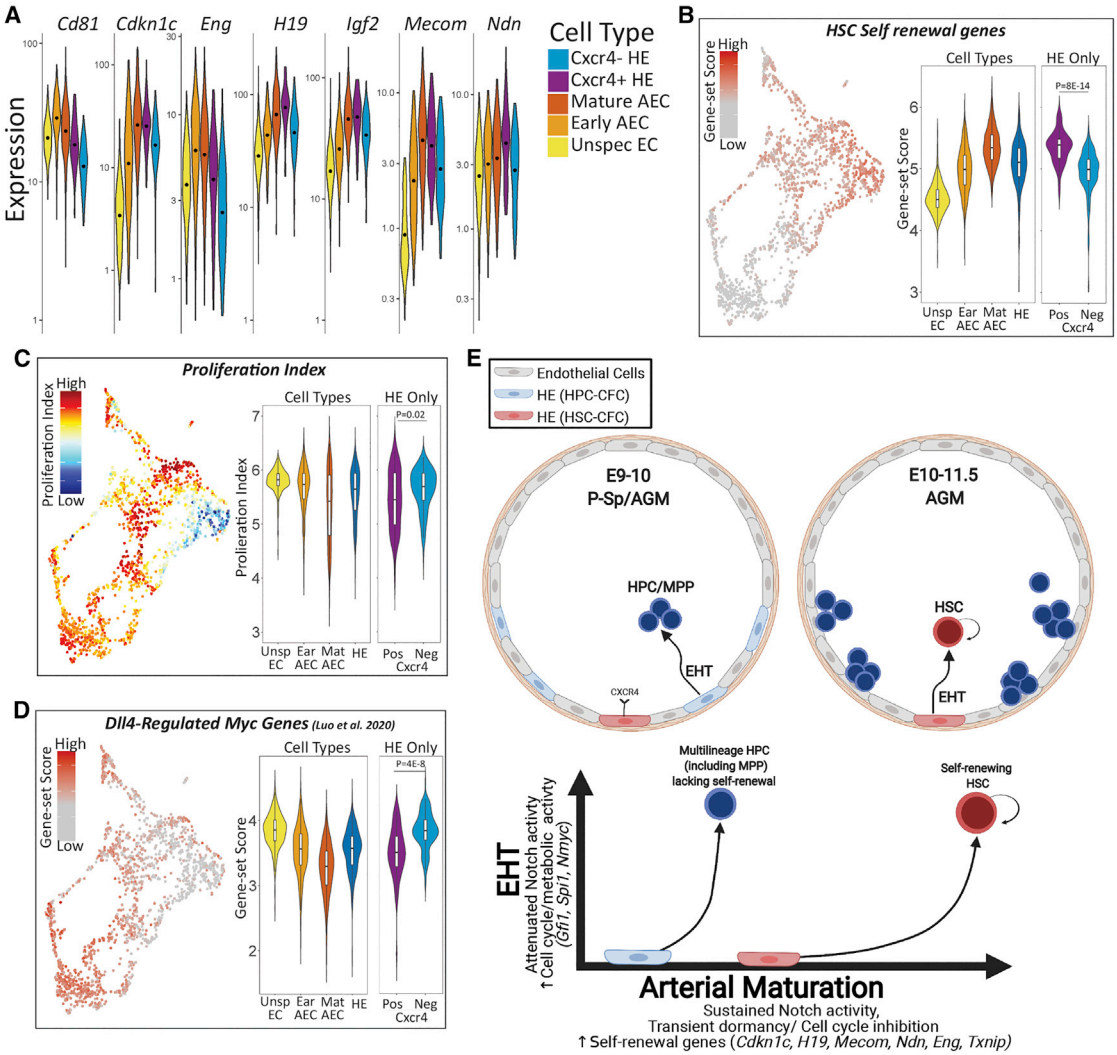

Figure 4. Acquisition of self-renewal programs defining HSC potential

(A) Violin plots of HSC self-renewal genes identified by differential gene expression between Cxcr4-positive and Cxcr4-negative HE.

(B) UMAP heatmap (left) and violin plots (right) of gene-set scores for published HSC self-renewal genes. p values indicate Wilcoxon rank-sum test.

(C) UMAP heatmap (left) and violin plots (right) of proliferation index. p values indicate Wilcoxon rank-sum test.

(D) UMAP heatmap (left) and violin plots (right) of gene-set scores for Dll4-regulated Myc pathway genes (Luo et al., 2021). p values indicate Wilcoxon rank-sum test.

(E) Model depicting distinct waves of multilineage progenitors and HSCs derived from HE distinguished by relative expression of genes driving self-renewal tied to arterial maturation and genes driving EHT. Image created with BioRender.

See also Figure S4 and Tables S3 and S4.

multilineage hematopoiesis during EHT in the E9–9.5 P-Sp/AGM rather than specific markers of HSC fate. In contrast, our data suggest that HSC competence is uniquely defined by the balanced expression of these HE-specific genes together with HSC self-renewal factors tied to arterial transcriptional programs, implying that the precise timing and dynamic modulation of signals promoting arterial maturation of HE and those driving EHT may be essential to enable HSC fate (Figure 4E).

Our results also suggest that transient dormancy characterized by delayed cell cycle entry and low metabolic activity may be a feature of HSC-competent HE in the early P-Sp/AGM, based on the lower expression of cell cycle and Myc pathway genes, and higher expression of known HSC cell cycle regulators such as *Mecom*, *Necdin*, and *Cdkn1c* (Asai et al., 2012; Kataoka et al., 2011; Kustikova et al., 2013; Matsumoto et al., 2011). This is consistent with studies in Fucci reporter mice, in which HSC precursor activity is restricted to cells in G_0/G_1 at E9.5 but is subsequently detected in actively cycling cells in the E10.5–11.5 AGM (Batsivari et al., 2017). Future studies are required to identify a precise mechanism linking metabolic and proliferative dormancy to HSC fate during HE specification. Interestingly, a reversible dormancy state mediated by Myc pathway inhibition has been implicated in embryonic diapause, maintenance of adult HSCs, and resistance of

cancer cells to chemotherapy, and Myc pathway inhibition was also recently shown to regulate arterial EC fate downstream of Dll4-Notch signaling (Cabezas-Wallscheid et al., 2017; Dhimolea et al., 2021; Duy et al., 2021; Luo et al., 2021; Scognamiglio et al., 2016). Notch signaling has also been implicated in arterial EC fate by promoting cell cycle arrest via a GJA4-CDKN1B axis downstream of blood flow (Fang et al., 2017), and CXCL12-CXCR4 signaling is also known to promote adult HSC quiescence (Nie et al., 2008), suggesting additional potential mechanisms. Interestingly, Porcheri et al. (2020) recently demonstrated a role for the Notch ligand DLL4 in inhibiting recruitment of HE to nascent intra-aortic hematopoietic clusters in the AGM. Combined with our current studies, this suggests a model in which DLL4-mediated Notch activation could transiently delay EHT from a subset of CXCR4-expressing HE in the E9–9.5 P-Sp, promoting further maturation of arterial programs that we show are closely associated with expression of HSC self-renewal/dormancy genes. This model would account for the sequential emergence of MPP/HPC activity in the E9–10 P-Sp that lack self-renewal/engraftment properties followed by a burst of pre-HSC/HSC activity peaking between E10.5 and E11.5 (Figure 4E; Hadland et al., 2021; Rybtsov et al., 2016). It further suggests the need for precise temporal modulation of Notch activity and downstream arterial-associated pathways to enable HSC fate, which may be critical for efforts to generate HSCs from PSCs. Altogether, our studies shift the current paradigm of developmental hematopoiesis by revealing a wave of MPPs that emerges from HE independently of HSCs, and they further provide insight into the transcriptional mechanisms of self-renewal acquisition required for HSC fate.

Limitations of the study and future directions

In the context of other recent studies discussed above, our results presented herein prompt several interesting hypotheses about how HE may acquire HSC competence, which will require future investigation. For one, our findings suggest that expression of a subset of genes essential for HSC maintenance and self-renewal are initially linked to arterial-specific transcriptional programs initiated in HE rather than transcriptional programs driving EHT and hematopoiesis. However, the molecular mechanisms regulating the expression of these genes, and whether these genes are regulated directly or indirectly by pathways that also control arterial EC fate, remain to be determined. For example, whether delaying EHT by transiently sustaining higher Notch activity and/or inhibiting Myc activity is sufficient to enhance HSC competence of HE must be tested directly; this will likely require fine-tuning of both the timing and activity level of these pathways during HE formation. Furthermore, whether CXCR4 is simply a marker of HSC-competent HE at this stage, or whether signaling through CXCR4 plays an important role in the acquisition of HSC competence, also requires further exploration, although prior studies in zebrafish and our own recent studies implicate CXCL12-CXCR4 signaling in embryonic HSC formation (Hadland et al., 2021; Nguyen et al., 2014; Pillay et al., 2016). Sorting out the mechanisms necessary to impart HSC competence to HE will be vital to establishing HSC engineering protocols for future translational applications.

STAR★METHODS

Detailed methods are provided in the online version of this paper and include the following:

- KEY RESOURCES TABLE
- RESOURCE AVAILABILITY
  - Lead contact
  - Materials availability
  - Data and code availability
- EXPERIMENTAL MODEL AND SUBJECT DETAILS
  - Mice
  - Cell lines
- METHOD DETAILS
  - Embryo dissections and cell sorting
  - AGM-EC co-culture
  - Flow cytometry analysis of cultured cells
  - Transplantation assays
  - Quantification of HSC and HPC colony-forming cells
  - Single-cell index analysis
  - HPC-CFC hematopoietic lineage potential assays
  - OP9 co-culture assay
  - Quantification of HPC-CFCs
  - Single-cell RNA sequencing
  - Single-cell transcriptome analysis and quality control
  - Dimensionality reduction, batch correction, and cluster analysis
  - Cell type classification
  - Gene-set scores
  - Pseudotime analysis
  - Gene module analysis
  - Differential gene expression
  - Gene Ontology (GO) analysis
- QUANTIFICATION AND STATISTICAL ANALYSIS

SUPPLEMENTAL INFORMATION

Supplemental information can be found online at https://doi.org/10.1016/j.celrep.2021.109675.

ACKNOWLEDGMENTS

This work was supported by the American Society of Hematology Scholar Award (to B.H.), the National Heart, Lung, and Blood Institute of the National Institutes of Health (NIH) (K08HL140143 to B.H.), and by the National Institute of Diabetes and Digestive and Kidney Diseases of the NIH (RC2DK114777 to I.D.B., C.T., S.R., and B.H.). This work was also supported by the Flow Cytometry shared resource of the Fred Hutch/University of Washington Cancer Consortium (NCI grant P30 CA015704). We would like to thank members of the Trapnell, Hadland, Bernstein, and Rafii labs for constructive feedback. The graphical abstract was created with BioRender.

AUTHOR CONTRIBUTIONS

Conceptualization, B.H., T.D., I.D.B., B.V.-F., S.R., and C.T.; methodology, B.H., T.D., I.D.B., B.V.-F., S.R., and C.T.; investigation, T.D., S.D., B.H., B.V.-F., S.S., O.W., A.H., D.J., T.I., and C.N.-M.; writing – original draft, T.D. and B.H.; writing – review & editing, all authors; funding acquisition, B.H., I.D.B., S.R., and C.T.; supervision, B.H.

DECLARATION OF INTERESTS

The authors declare no competing interests.

Received: April 13, 2021
Revised: June 28, 2021
Accepted: August 16, 2021
Published: September 14, 2021

REFERENCES

Aranguren, X.L., Agirre, X., Beerens, M., Coppiello, G., Uriz, M., Vandersmissen, I., Benkheil, M., Panadero, J., Aguado, N., Pascual-Montano, A., et al. (2013). Unraveling a novel transcription factor code determining the human arterial-specific endothelial cell signature. Blood *122*, 3982–3992.

Asai, T., Liu, Y., Di Giandomenico, S., Bae, N., Ndiaye-Lobry, D., Deblasio, A., Menendez, S., Antipin, Y., Reva, B., Wevrick, R., and Nimer, S.D. (2012). Necdin, a p53 target gene, regulates the quiescence and response to genotoxic stress of hematopoietic stem/progenitor cells. Blood *120*, 1601–1612.

Ashburner, M., Ball, C.A., Blake, J.A., Botstein, D., Butler, H., Cherry, J.M., Davis, A.P., Dolinski, K., Dwight, S.S., Eppig, J.T., et al.; The Gene Ontology Consortium (2000). Gene ontology: tool for the unification of biology. Nat. Genet. *25*, 25–29.

Batsivari, A., Rybtsov, S., Souilhol, C., Binagui-Casas, A., Hills, D., Zhao, S., Travers, P., and Medvinsky, A. (2017). Understanding hematopoietic stem cell development through functional correlation of their proliferative status with the intra-aortic cluster architecture. Stem Cell Reports *8*, 1549–1562.

Böiers, C., Carrelha, J., Lutteropp, M., Luc, S., Green, J.C., Azzoni, E., Woll, P.S., Mead, A.J., Hultquist, A., Swiers, G., et al. (2013). Lymphomyeloid contribution of an immune-restricted progenitor emerging prior to definitive hematopoietic stem cells. Cell Stem Cell *13*, 535–548.

Borges, L., Oliveira, V.K.P., Baik, J., Bendall, S.C., and Perlingeiro, R.C.R. (2019). Serial transplantation reveals a critical role for endoglin in hematopoietic stem cell quiescence. Blood *133*, 688–696.

Boroviak, T., Loos, R., Lombard, P., Okahara, J., Behr, R., Sasaki, E., Nichols, J., Smith, A., and Bertone, P. (2015). Lineage-specific profiling delineates the emergence and progression of naive pluripotency in mammalian embryogenesis. Dev. Cell *35*, 366–382.

Cabezas-Wallscheid, N., Buettner, F., Sommerkamp, P., Klimmeck, D., Ladel, L., Thalheimer, F.B., Pastor-Flores, D., Roma, L.P., Renders, S., Zeisberger, P., et al. (2017). Vitamin a-retinoic acid signaling regulates hematopoietic stem cell dormancy. Cell *169*, 807–823.e19.

Cao, J., Spielmann, M., Qiu, X., Huang, X., Ibrahim, D.M., Hill, A.J., Zhang, F., Mundlos, S., Christiansen, L., Steemers, F.J., et al. (2019). The single-cell transcriptional landscape of mammalian organogenesis. Nature *566*, 496–502.

Carbon, S., Ireland, A., Mungall, C.J., Shu, S., Marshall, B., and Lewis, S.AmiGO Hub; Web Presence Working Group (2009). AmiGO: Online access to ontology and annotation data. Bioinformatics *25*, 288–289.

Chambers, S.M., Boles, N.C., Lin, K.Y., Tierney, M.P., Bowman, T.V., Bradfute, S.B., Chen, A.J., Merchant, A.A., Sirin, O., Weksberg, D.C., et al. (2007). Hematopoietic fingerprints: an expression database of stem cells and their progeny. Cell Stem Cell *1*, 578–591.

de Bruijn, M.F., Speck, N.A., Peeters, M.C., and Dzierzak, E. (2000). Definitive hematopoietic stem cells first develop within the major arterial regions of the mouse embryo. EMBO J. *19*, 2465–2474.

Dhimolea, E., de Matos Simoes, R., Kansara, D., Al'Khafaji, A., Bouyssou, J., Weng, X., Sharma, S., Raja, J., Awate, P., Shirasaki, R., et al. (2021). An embryonic diapause-like adaptation with suppressed Myc activity enables tumor treatment persistence. Cancer Cell *39*, 240–256.e11.

Ditadi, A., Sturgeon, C.M., Tober, J., Awong, G., Kennedy, M., Yzaguirre, A.D., Azzola, L., Ng, E.S., Stanley, E.G., French, D.L., et al. (2015). Human definitive haemogenic endothelium and arterial vascular endothelium represent distinct lineages. Nat. Cell Biol. *17*, 580–591.

Duy, C., Li, M., Teater, M., Meydan, C., Garrett-Bakelman, F.E., Lee, T.C., Chin, C.R., Durmaz, C., Kawabata, K.C., Dhimolea, E., et al. (2021). Chemotherapy induces senescence-like resilient cells capable of initiating AML recurrence. Cancer Discov. *11*, 1542–1561.

Fang, J.S., Coon, B.G., Gillis, N., Chen, Z., Qiu, J., Chittenden, T.W., Burt, J.M., Schwartz, M.A., and Hirschi, K.K. (2017). Shear-induced Notch-Cx37-p27 axis arrests endothelial cell cycle to enable arterial specification. Nat. Commun. *8*, 2149.

Ficara, F., Murphy, M.J., Lin, M., and Cleary, M.L. (2008). Pbx1 regulates self-renewal of long-term hematopoietic stem cells by maintaining their quiescence. Cell Stem Cell *2*, 484–496.

Frelin, C., Herrington, R., Janmohamed, S., Barbara, M., Tran, G., Paige, C.J., Benveniste, P., Zuñiga-Pflücker, J.C., Souabni, A., Busslinger, M., and Iscove, N.N. (2013). GATA-3 regulates the self-renewal of long-term hematopoietic stem cells. Nat. Immunol. *14*, 1037–1044.

Fridman, A.L., and Tainsky, M.A. (2008). Critical pathways in cellular senescence and immortalization revealed by gene expression profiling. Oncogene *27*, 5975–5987.

Gene Ontology Consortium (2021). The Gene Ontology resource: Enriching a GOld mine. Nucleic Acids Res. *49* (*D1*), D325–D334.

Goyama, S., Yamamoto, G., Shimabe, M., Sato, T., Ichikawa, M., Ogawa, S., Chiba, S., and Kurokawa, M. (2008). Evi-1 is a critical regulator for hematopoietic stem cells and transformed leukemic cells. Cell Stem Cell *3*, 207–220.

Hadland, B., and Yoshimoto, M. (2018). Many layers of embryonic hematopoiesis: New insights into B-cell ontogeny and the origin of hematopoietic stem cells. Exp. Hematol. *60*, 1–9.

Hadland, B.K., Varnum-Finney, B., Poulos, M.G., Moon, R.T., Butler, J.M., Rafii, S., and Bernstein, I.D. (2015). Endothelium and NOTCH specify and amplify aorta-gonad-mesonephros-derived hematopoietic stem cells. J. Clin. Invest. *125*, 2032–2045.

Hadland, B.K., Varnum-Finney, B., Mandal, P.K., Rossi, D.J., Poulos, M.G., Butler, J.M., Rafii, S., Yoder, M.C., Yoshimoto, M., and Bernstein, I.D. (2017). A common origin for B-1a and B-2 lymphocytes in clonal pre- hematopoietic stem cells. Stem Cell Reports *8*, 1563–1572.

Hadland, B.K., Varnum-Finney, B., Nourigat-Mckay, C., Flowers, D., and Bernstein, I.D. (2018). Clonal analysis of embryonic hematopoietic stem cell precursors using single cell index sorting combined with endothelial cell niche co-culture. J. Vis. Exp. (*135*), 56973.

Hadland, B., Varnum-Finney, B., Dozono, S., Dignum, T., Nourigat-McKay, C., Jackson, D.L., Itkin, T., Butler, J.M., Rafii, S., Trapnell, C., and Bernstein, I.D. (2021). Engineering a niche supporting haematopoietic stem cell development using integrated single cell transcriptomics. bioRxiv. https://doi.org/10.1101/2021.01.25.427999.

Haghverdi, L., Lun, A.T.L., Morgan, M.D., and Marioni, J.C. (2018). Batch effects in single-cell RNA-sequencing data are corrected by matching mutual nearest neighbors. Nat. Biotechnol. *36*, 421–427.

Hou, S., Li, Z., Zheng, X., Gao, Y., Dong, J., Ni, Y., Wang, X., Li, Y., Ding, X., Chang, Z., et al. (2020). Embryonic endothelial evolution towards first hematopoietic stem cells revealed by single-cell transcriptomic and functional analyses. Cell Res. *30*, 376–392.

Huang, W., Sherman, B.T., and Lempicki, R.A. (2009a). Bioinformatics enrichment tools: Paths toward the comprehensive functional analysis of large gene lists. Nucleic Acids Res. *37*, 1–13.

Huang, W., Sherman, B.T., and Lempicki, R.A. (2009b). Systematic and integrative analysis of large gene lists using DAVID bioinformatics resources. Nat. Protoc. *4*, 44–57.

Inlay, M.A., Serwold, T., Mosley, A., Fathman, J.W., Dimov, I.K., Seita, J., and Weissman, I.L. (2014). Identification of multipotent progenitors that emerge prior to hematopoietic stem cells in embryonic development. Stem Cell Reports *2*, 457–472.

Iturri, L., Freyer, L., Biton, A., Dardenne, P., Lallemand, Y., and Gomez Perdiguero, E. (2021). Megakaryocyte production is sustained by direct differentiation from erythromyeloid progenitors in the yolk sac until midgestation. Immunity *54*, 1433–1446.e5.

Jankovic, V., Ciarrocchi, A., Boccuni, P., DeBlasio, T., Benezra, R., and Nimer, S.D. (2007). Id1 restrains myeloid commitment, maintaining the self-renewal capacity of hematopoietic stem cells. Proc. Natl. Acad. Sci. USA *104*, 1260–1265.

Jeong, M., Piao, Z.H., Kim, M.S., Lee, S.H., Yun, S., Sun, H.N., Yoon, S.R., Chung, J.W., Kim, T.D., Jeon, J.H., et al. (2009). Thioredoxin-interacting protein regulates hematopoietic stem cell quiescence and mobilization under stress conditions. J. Immunol. *183*, 2495–2505.

Jude, C.D., Climer, L., Xu, D., Artinger, E., Fisher, J.K., and Ernst, P. (2007). Unique and independent roles for MLL in adult hematopoietic stem cells and progenitors. Cell Stem Cell *1*, 324–337.

Kataoka, K., Sato, T., Yoshimi, A., Goyama, S., Tsuruta, T., Kobayashi, H., Shimabe, M., Arai, S., Nakagawa, M., Imai, Y., et al. (2011). Evi1 is essential for hematopoietic stem cell self-renewal, and its expression marks hematopoietic cells with long-term multilineage repopulating activity. J. Exp. Med. *208*, 2403–2416.

Kustikova, O.S., Schwarzer, A., Stahlhut, M., Brugman, M.H., Neumann, T., Yang, M., Li, Z., Schambach, A., Heinz, N., Gerdes, S., et al. (2013). Activation of *Evi1* inhibits cell cycle progression and differentiation of hematopoietic progenitor cells. Leukemia *27*, 1127–1138.

Lin, K.K., Rossi, L., Boles, N.C., Hall, B.E., George, T.C., and Goodell, M.A. (2011). CD81 is essential for the re-entry of hematopoietic stem cells to quiescence following stress-induced proliferation via deactivation of the Akt pathway. PLoS Biol. *9*, e1001148.

Luo, W., Garcia-Gonzalez, I., Fernández-Chacón, M., Casquero-Garcia, V., Sanchez-Muñoz, M.S., Mühleder, S., Garcia-Ortega, L., Andrade, J., Potente, M., and Benedito, R. (2021). Arterialization requires the timely suppression of cell growth. Nature *589*, 437–441.

Mallaney, C., Ostrander, E.L., Celik, H., Kramer, A.C., Martens, A., Kothari, A., Koh, W.K., Haussler, E., Iwamori, N., Gontarz, P., et al. (2019). Kdm6b regulates context-dependent hematopoietic stem cell self-renewal and leukemogenesis. Leukemia *33*, 2506–2521.

Matsumoto, A., Takeishi, S., Kanie, T., Susaki, E., Onoyama, I., Tateishi, Y., Nakayama, K., and Nakayama, K.I. (2011). p57 is required for quiescence and maintenance of adult hematopoietic stem cells. Cell Stem Cell *9*, 262–271.

McMahon, K.A., Hiew, S.Y., Hadjur, S., Veiga-Fernandes, H., Menzel, U., Price, A.J., Kioussis, D., Williams, O., and Brady, H.J. (2007). Mll has a critical role in fetal and adult hematopoietic stem cell self-renewal. Cell Stem Cell *1*, 338–345.

Medvinsky, A., and Dzierzak, E. (1996). Definitive hematopoiesis is autonomously initiated by the AGM region. Cell *86*, 897–906.

Müller, A.M., Medvinsky, A., Strouboulis, J., Grosveld, F., and Dzierzak, E. (1994). Development of hematopoietic stem cell activity in the mouse embryo. Immunity *1*, 291–301.

Nguyen, P.D., Hollway, G.E., Sonntag, C., Miles, L.B., Hall, T.E., Berger, S., Fernandez, K.J., Gurevich, D.B., Cole, N.J., Alaei, S., et al. (2014). Haematopoietic stem cell induction by somite-derived endothelial cells controlled by *meox1*. Nature *512*, 314–318.

Nie, Y., Han, Y.C., and Zou, Y.R. (2008). CXCR4 is required for the quiescence of primitive hematopoietic cells. J. Exp. Med. *205*, 777–783.

Oatley, M., Bölükbası, Ö.V., Svensson, V., Shvartsman, M., Ganter, K., Zirngibl, K., Pavlovich, P.V., Milchevskaya, V., Foteva, V., Natarajan, K.N., et al. (2020). Single-cell transcriptomics identifies CD44 as a marker and regulator of endothelial to haematopoietic transition. Nat. Commun. *11*, 586.

Palis, J. (2016). Hematopoietic stem cell-independent hematopoiesis: emergence of erythroid, megakaryocyte, and myeloid potential in the mammalian embryo. FEBS Lett. *590*, 3965–3974.

Pillay, L.M., Mackowetzky, K.J., Widen, S.A., and Waskiewicz, A.J. (2016). Somite-derived retinoic acid regulates zebrafish hematopoietic stem cell formation. PLoS ONE *11*, e0166040.

Pliner, H.A., Shendure, J., and Trapnell, C. (2019). Supervised classification enables rapid annotation of cell atlases. Nat. Methods *16*, 983–986.

Porcheri, C., Golan, O., Calero-Nieto, F.J., Thambyrajah, R., Ruiz-Herguido, C., Wang, X., Catto, F., Guillén, Y., Sinha, R., González, J., et al. (2020). Notch ligand Dll4 impairs cell recruitment to aortic clusters and limits blood stem cell generation. EMBO J. *39*, e104270.

Rodriguez-Fraticelli, A.E., Weinreb, C., Wang, S.W., Migueles, R.P., Jankovic, M., Usart, M., Klein, A.M., Lowell, S., and Camargo, F.D. (2020). Single-cell lineage tracing unveils a role for TCF15 in haematopoiesis. Nature *583*, 585–589.

Rybtsov, S., Ivanovs, A., Zhao, S., and Medvinsky, A. (2016). Concealed expansion of immature precursors underpins acute burst of adult HSC activity in foetal liver. Development *143*, 1284–1289.

Schmitt, T.M., and Zúñiga-Pflücker, J.C. (2006). T-cell development, doing it in a dish. Immunol. Rev. *209*, 95–102.

Scognamiglio, R., Cabezas-Wallscheid, N., Thier, M.C., Altamura, S., Reyes, A., Prendergast, Á.M., Baumgärtner, D., Carnevalli, L.S., Atzberger, A., Haas, S., et al. (2016). Myc depletion induces a pluripotent dormant state mimicking diapause. Cell *164*, 668–680.

Soares-da-Silva, F., Freyer, L., Elsaid, R., Burlen-Defranoux, O., Iturri, L., Sismeiro, O., Pinto-do-Ó, P., Gomez-Perdiguero, E., and Cumano, A. (2021). Yolk sac, but not hematopoietic stem cell-derived progenitors, sustain erythropoiesis throughout murine embryonic life. J. Exp. Med. *218*, e20201729.

Srivatsan, S.R., McFaline-Figueroa, J.L., Ramani, V., Saunders, L., Cao, J., Packer, J., Pliner, H.A., Jackson, D.L., Daza, R.M., Christiansen, L., et al. (2020). Massively multiplex chemical transcriptomics at single-cell resolution. Science *367*, 45–51.

Taoudi, S., Bee, T., Hilton, A., Knezevic, K., Scott, J., Willson, T.A., Collin, C., Thomas, T., Voss, A.K., Kile, B.T., et al. (2011). ERG dependence distinguishes developmental control of hematopoietic stem cell maintenance from hematopoietic specification. Genes Dev. *25*, 251–262.

Thomas, D.D., Sommer, A.G., Balazs, A.B., Beerman, I., Murphy, G.J., Rossi, D., and Mostoslavsky, G. (2016). Insulin-like growth factor 2 modulates murine hematopoietic stem cell maintenance through upregulation of p57. Exp. Hematol. *44*, 422–433.e1.

Tirosh, I., Izar, B., Prakadan, S.M., Wadsworth, M.H., 2nd, Treacy, D., Trombetta, J.J., Rotem, A., Rodman, C., Lian, C., Murphy, G., et al. (2016). Dissecting the multicellular ecosystem of metastatic melanoma by single-cell RNA-seq. Science *352*, 189–196.

Trapnell, C., Cacchiarelli, D., Grimsby, J., Pokharel, P., Li, S., Morse, M., Lennon, N.J., Livak, K.J., Mikkelsen, T.S., and Rinn, J.L. (2014). The dynamics and regulators of cell fate decisions are revealed by pseudotemporal ordering of single cells. Nat. Biotechnol. *32*, 381–386.

Venkatraman, A., He, X.C., Thorvaldsen, J.L., Sugimura, R., Perry, J.M., Tao, F., Zhao, M., Christenson, M.K., Sanchez, R., Yu, J.Y., et al. (2013). Maternal imprinting at the *H19-Igf2* locus maintains adult haematopoietic stem cell quiescence. Nature *500*, 345–349.

Vink, C.S., Calero-Nieto, F.J., Wang, X., Maglitto, A., Mariani, S.A., Jawaid, W., Göttgens, B., and Dzierzak, E. (2020). Iterative single-cell analyses define the transcriptome of the first functional hematopoietic stem cells. Cell Rep. *31*, 107627.

Wang, H., Diao, D., Shi, Z., Zhu, X., Gao, Y., Gao, S., Liu, X., Wu, Y., Rudolph, K.L., Liu, G., et al. (2016). SIRT6 controls hematopoietic stem cell homeostasis through epigenetic regulation of Wnt signaling. Cell Stem Cell *18*, 495–507.

Wilson, N.K., Kent, D.G., Buettner, F., Shehata, M., Macaulay, I.C., Calero-Nieto, F.J., Sánchez Castillo, M., Oedekoven, C.A., Diamanti, E., Schulte, R., et al. (2015). Combined single-cell functional and gene expression analysis resolves heterogeneity within stem cell populations. Cell Stem Cell *16*, 712–724.

Xu, C., Gao, X., Wei, Q., Nakahara, F., Zimmerman, S.E., Mar, J., and Frenette, P.S. (2018). Stem cell factor is selectively secreted by arterial endothelial cells in bone marrow. Nat. Commun. *9*, 2449.

Zhu, Q., Gao, P., Tober, J., Bennett, L., Chen, C., Uzun, Y., Li, Y., Howell, E.D., Mumau, M., Yu, W., et al. (2020). Developmental trajectory of prehematopoietic stem cell formation from endothelium. Blood *136*, 845–856.

STAR★METHODS

KEY RESOURCES TABLE

REAGENT or RESOURCE	SOURCE	IDENTIFIER
Antibodies		
CD201 (EPCR) Anti-mouse Monoclonal Antibody PerCP-eFluor710 Clone eBio1560	eBioscience	Cat#46-2012-80; RRID:AB_10718383
CD61 Anti-mouse/rat Monoclonal Antibody APC Clone 2C9.G2	Biolegend	Cat#104316; RRID:AB_2561734
CD144 (VE-cadherin) Anti-mouse Monoclonal Antibody PE-Cyanine7 Clone eBioBV13	eBioscience	Cat#25-1441-82; RRID:AB_2573402
CD45 Anti-mouse Monoclonal Antibody FITC Clone 30-F11	eBioscience	Cat#11-0451-85; RRID:AB_465051
CD184 (CXCR4) Anti-mouse Monoclonal Antibody PE Clone 2B11	Invitrogen	Cat#12-9991-81; RRID:AB_891393
CD41 Anti-mouse Monoclonal Antibody FITC Clone MWReg30	BD Biosciences	Cat#553848; RRID:AB_395085
CD43 Anti-mouse Monoclonal Antibody FITC Clone eBioR2/60	eBioscience	Cat#11-0431-82; RRID:AB_465040
CD44 Anti-mouse Monoclonal Antibody APC Clone IM7	eBioscience	Cat#17-0441-82; RRID:AB_469390
Rat IgG2b kappa Isotype Control Antibody PE Clone A95-1	BD PharMingen	Cat#553989; RRID:AB_10049479
Rat IgG1 kappa Isotype Control Antibody FITC Clone R3-34	BD PharMingen	Cat#553924; RRID:AB_479706
Rat IgM kappa Isotype Control Antibody FITC Clone eBRM	eBioscience	Cat#11-4341-82; RRID:AB_470017
Rat IgG2b kappa Isotype Control Antibody FITC Clone A95-1	BD PharMingen	Cat#553988; RRID:AB_479619
Rat IgG2b kappa Isotype Control Antibody APC Clone A95-1	BD PharMingen	Cat#553991; RRID:AB_10050405
DLL4 Anti-mouse Mononclonal Antibody PE Clone HMD4-1	Biolegend	Cat#130808; RRID:AB_2092983
Armenian Hamster IgG Isotype Control Antibody PE Clone eBio299Arm	eBioscience	Cat#12-4888-81; RRID:AB_470073
Ly-6G and LY6C (Gr-1) Rat Anti-mouse Monoclonal Antibody FITC Clone RB6-8C5	BD PharMingen	Cat#553127; RRID:AB_394643
F4/80 Anti-mouse Monoclonal Antibody FITC Clone BM8	eBioscience	Cat#553127; RRID:AB_2637191
CD45 Anti-mouse Monoclonal Antibody PerCP-Cyanine5.5 Clone 30-F11	eBioscience	Cat#45-0451-82; RRID:AB_1107002
CD201 (EPCR) Anti-mouse Monoclonal Antibody PE Clone eBio1560	eBioscience	Cat#12-2012-82; RRID:AB_914317
Ly-6A/E (Sca-1) Anti-mouse Monoclonal Antibody APC Clone D7	eBioscience	Cat#17-5981-82; RRID:AB_469487
CD93 (AA4.1) Anti-mouse Monoclonal Antibody PE Clone AA4.1	eBioscience	Cat#12-5892-81; RRID:AB_466017
CD19 Anti-mouse Monoclonal Antibody APC Clone 1D3	BD PharMingen	Cat#550992; RRID:AB_398483
CD45R (B220) Ant-mouse Monoclonal Antibody PerCP Clone RAB-6B2	BD PharMingen	Cat#553093; RRID:AB_394622

(*Continued on next page*)

Continued

REAGENT or RESOURCE	SOURCE	IDENTIFIER
CD11b Anti-mouse Monoclonal Antibody APC-eFluor780 Clone M1/70	eBioscience	Cat#47-011282; RRID:AB_1603193
CD8a Anti-mouse Monoclonal Antibody PE Clone 53-6.7	BD PharMingen	Cat#553033; RRID:AB_394571
CD4 Anti-mouse Monoclonal Antibody PerCP Clone RM4-5	BD PharMingen	Cat#553052; RRID:AB_394587
CD25 Anti-mouse Monoclonal Antibody PE-Cyanine7 Clone PC61	BD PharMingen	Cat#552880; RRID:AB_394509
Rat IgG2a kappa Isotype Control Antibody PerCP Clone R35-95	BD PharMingen	Cat#553933; RRID:AB_10056901
Rat IgG2b kappa Isotype Control Antibody APC-Cy7 Clone A95-1	BD PharMingen	Cat#552773; RRID:AB_394459
Rat IgG1 kappa Isotype Control Antibody PE-Cyanine7, Clone eBRG1	eBioscience	Cat#25-4301-82; RRID:AB_470198
Rat IgG2a kappa Isotype Control Antibody PE Clone eBR2a	eBioscience	Cat#12-4321-80; RRID:AB_1834380
Rat IgG2b kappa Isotype Control Antibody PerCP-Cyanine5.5 Clone RTK4530	Biolegend	Cat#400632; RRID:AB_893677
Rat IgG2a kappa Isotype Control Antibody APC Clone R35-95	BD PharMingen	Cat#553932; RRID:AB_479720
Rat IgG2a kappa Isotype Control Antibody APC-eFluor 780 Clone eBR2a	eBioscience	Cat#47-4321-82; RRID:AB_11063700
CD45.1 Anti-mouse Monoclonal Antibody PE-Cyanine7 Clone A20	eBioscience	Cat#25-0453-82; RRID:AB_469629
CD45.2 Anti-mouse Monoclonal Antibody APC-eFluor 780 Clone 104	eBioscience	Cat#47-0454-82; RRID:AB_1272175
CD3 Rat Anti-Mouse Monoclonal Antibody FITC Clone 17A2	BD PharMingen	Cat#555274; RRID:AB_395698
F4/80 Anti-mouse Monoclonal Antibody PE Clone BM8	Biolegend	Cat#123110; RRID:AB_893486
Ly-6G and Ly-6C (Gr-1) Rat Anti-Mouse PerCP-Cyanine5.5 Clone RB6-8C5	BD PharMingen	Cat#552093; RRID:AB_394334
CD19 Anti-Mouse Monoclonal Antibody APC Clone 1D3	Biolegend	Cat#152410; RRID:AB_2629839
Chemicals, peptides, and recombinant proteins		
X-Vivo20	Lonza	Cat#04-448Q
Recombinant Murine SCF	Peprotech	Cat#250-03
Recombinant Murine IL-3	Peprotech	Cat#213-13
Recombinant Human TPO	Preprotech	Cat#300-18
Human Flt3-Ligand	Miltenyi Biotec	Cat#130-096-479
Human IL7	Miltenyi Biotec	Cat#130-095-363
Fetal Bovine Serum	ThermoFisher	Special order characterized lot
Dulbecco's Phosphate Buffered Saline (PBS)	GIBCO	Cat#14190-144
Collagenase Type 1 (0.25%)	Stemcell Technologies	Cat#07902
Anti-mouse CD16/32 (FcR block)	BD Biosciences	Cat#553141
MEM alpha	GIBCO	Cat# 12561056
Penicillin/StreptoMycin (100X)	GIBCO	Cat# 15140-122
TrypLE Express	GIBCO	Cat#12605-028
Methocult GF M3434	Stemcell Technologies	Cat#03434
EmbryoMax 0.1% Gelatin solution	MilliporeSigma	Cat#ES006B

(*Continued on next page*)

Continued

REAGENT or RESOURCE	SOURCE	IDENTIFIER
DAPI	Millipore	Cat#268298
Iscove's Modified Dulbecco's Medium (IMDM)	GIBCO	Cat#12440-053
Heparin	Sigma	Cat# H3149-100KU
L-Glutamine	Stemcell Technologies	Cat#7100
Endothelial Mitogen *No longer available—substitute with rm VEGF, rm FGF, rm IGF, rm EGF	Alfa Aesar	Cat#BT-203
Recombinant Murine VEGF	Peprotech	Cat# 450-32
Recombinant Murine FGF	Peprotech	Cat# 450-33
Recombinant Murine IGF	Peprotech	Cat# 250-19
Recombinant Murine EGF	Peprotech	Cat# 315-09
Critical commercial assays		
Chromium Single Cell 3′ GEM, Library & Gel Bead Kit v2	10X Genomics	Cat#120237
Chromium Single Cell B Chip Kit	10X Genomics	Cat#1000073
Chromium i7 Multiplex Kit	10X Genomics	Cat#120262
Illumina NextSeq 550 high-output kit	Illumina	
24-well tissue culture plates	Fisher Scientific	Cat#0720084
96-well tissue culture plates	Fisher Scientific	Cat#0720092
48-well tissue culture plates	Fisher Scientific	Cat#0877252
Deposited data		
Single Cell RNA Seq Data	This paper	NCBI GEO: GSE171457
Code	This paper	Github repository: https://github.com/FredHutch/dignum-etal-2021. Zenodo: https://zenodo.org/record/5153974#.YQg8cW5lD0o
Experimental models: Cell lines		
AGM-EC	Hadland lab	https://protocolexchange.researchsquare.com/article/pex-986/v1
OP9-Dll4 cell line	Zúñiga-Pflücker lab	N/A
OP9-GFP cell line	Zúñiga-Pflücker lab	N/A
Experimental models: Organisms/strains		
Mouse: C57BL/6J	Bred in house (origination: Jackson laboratories)	N/A
Mouse: C57BL/6.SJL-Ly5.1-Pep3b	Bred in house (origination: Jackson laboratories)	N/A
Software and algorithms		
monocle3 (v.3.2.3.0)	Cao et al., 2019	https://cole-trapnell-lab.github.io/monocle3/
ggplot2 (v 3.3.2)		https://ggplot2.tidyverse.org/
R (version 3.6.1)		https://www.r-project.org/
FlowJo (version 9, version 10.7.1)		https://www.flowjo.com/solutions/flowjo/downloads/previous-versions
CellRanger (v 2.1.1)		https://support.10xgenomics.com/single-cell-gene-expression/software/pipelines/latest/installation
garnett (v 0.2.15)	Pliner et al., 2019	https://cole-trapnell-lab.github.io/garnett/
ggpubr (v 0.4.0)		https://rdrr.io/cran/ggpubr/

RESOURCE AVAILABILITY

Lead contact

Further information and requests for resources and reagents should be directed to and will be fulfilled by the lead contact, Brandon Hadland (bhadland@fredhutch.org).

Materials availability

This study did not generate new unique reagents. We are happy to provide AGM-EC upon request.

Data and code availability

- Raw sequencing data and Monocle 3 cell datasets have been deposited at NCBI GEO: GSE171457 and are publicly available as of the date of publication.
- All original code generated during this study has been deposited at Github and is publicly available as of the date of publication. Github repository: https://github.com/FredHutch/dignum-etal-2021; Zenodo: https://zenodo.org/record/5153974#.YQg8cW5lD0o.
- Any additional information required to reanalyze the data reported in this paper is available from the lead contact upon request.

EXPERIMENTAL MODEL AND SUBJECT DETAILS

Mice

Wild-type C57Bl6/J7 (CD45.2) and congenic C57BL/6.SJL-Ly5.1-Pep3b (CD45.1) mice were bred at the Fred Hutchinson Cancer Research Center. Male and female C57Bl6/J7 CD45.2 mice at 8-12 weeks of age were used for timed matings and transplantation experiments. All animal studies were conducted in accordance with the NIH guidelines for humane treatment of animals and were approved by the Institutional Animal Care and Use Committee at the Fred Hutchinson Cancer Research Center.

Cell lines

AGM-derived Akt-ECs (AGM-ECs)

AGM-EC were generated as previously described (Hadland et al., 2015) and further detailed in a protocol available at Nature Protocol Exchange (https://protocolexchange.researchsquare.com/). For reproducibility, AGM-EC from frozen aliquots of the same derivation were used for all co-culture experiments at less than passage 15 for experiments in this manuscript. AGM-EC were plated at a density of $5X10^5$ cells/flask in gelatinized, tissue culture T75 flasks in EC media (consisting of IMDM with 20% FBS, Penicillin/streptoMycin, Heparin, L-glutamine, and EC mitogen*), and passaged every 3-4 days when confluent.

*EC mitogen no longer available (see STAR Key Resources Table for details on substitutes)

OP9/OP9-DLL4 stromal cells (OP9 cells)

GFP-expressing OP9 bone marrow stromal cells and GFP-expressing OP9 bone marrow stromal cells ectopically expressing Delta-like 4 (OP9-DLL4 cells) generated by the Zúñiga-Pflücker lab (Schmitt and Zúñiga-Pflücker, 2006) were used to assay the B- and T-lymphoid potential of hematopoietic colony cells. OP9 cell lines were plated at a density of $1.6X10^5$ cells/flask in gelatinized, tissue culture T25 flasks in OP9 media (consisting of aMEM with 20% FBS, and Penicillin/streptoMycin). Cells were passaged every 3 days (or when confluent) and used at passage numbers below 13 for co-culture assays.

METHOD DETAILS

Embryo dissections and cell sorting

Embryonic P-Sp/AGM regions were dissected from embryos harvested from pregnant C57Bl6/J7 (CD45.2) female mice as previously described (Hadland et al., 2015). Embryo age was precisely timed by counting somite pairs (sp), defined as follows (except where more specifically indicated in the figures): E9 (13-20sp), E9.5 (21-29 sp), and E10 (30-39sp). Dissected P-Sp/AGM tissues were treated with 0.25% collagenase for 25 minutes at 37°C, pipetted to single cell suspension, and washed with PBS containing 10% FBS. Cells were pre-incubated with anti-mouse CD16/CD32 (FcRII block) and stained with monoclonal antibodies as indicated. A detailed list of all antibodies used is shown in the STAR Key Resources Table. For most experiments, to isolate hemogenic endothelial populations, a combination of anti-mouse VE-Cadherin-PECy7, EPCR/CD201-PerCP-eFluor710, and/or CD61-APC were used, with or without additional anti-mouse antibodies CXCR4 (PE), CD41 (FITC), CD43 (FITC), CD45 (FITC), and CD44 (APC), as indicated in the results section. Relevant isotype control antibodies were used to set gates. DAPI staining was used to gate out dead cells. All reagents for cell staining were diluted in PBS with 10% FBS and staining was carried out on ice or at 4°C. Cells were sorted on a BD FACSAria II equipped with BD FACSDiva Software with index sorting capability. For index-sorted single cells, sorting was performed in single cell mode with maximum purity mask settings to minimize contaminating cells.

AGM-EC co-culture

For co-culture experiments, AGM-EC at passage 15 or less were plated 24-48 hours prior to initiation of co-culture at a density of $1X10^4$ cells per well to gelatin-treated 96-well tissue culture plates for single cell index co-culture or $4X10^4$ cells per 24-well for bulk co-culture. For single cell index co-culture, AGM-derived hemogenic cells were individually index sorted to each well of 96-well containing AGM-EC in serum-free media consisting of X-vivo 20 with recombinant cytokines: stem cell factor (SCF) and FMS-like tyrosine kinase 3 ligand (FLT3L) each at 100 ng/ml, and interleukin-3 (IL-3) and thrombopoietin (TPO) each at 20 ng/ml. Following 6 to 7 days of co-culture, each well was visualized for hematopoietic colony formation and 50% of cells were harvested by vigorous pipetting for phenotypic analysis by flow cytometry, and in some experiments, remaining cells were used for confirmatory transplantation assay as previously described (Hadland et al., 2017; Hadland et al., 2018) and/or secondary hematopoietic lineage potential assays (CFU assay and OP9 co-culture, described below). For co-culture of bulk populations, sorted cells were re-suspended in serum-free X-vivo 20 culture media with cytokines (excluding FLT3L) and plated at 3-5 embryo equivalent of cells per 24-well containing AGM-EC. Following 6 to 7 days of co-culture, hematopoietic progeny were harvested by vigorous pipetting for subsequent analysis by flow cytometry and transplantation assays, as described below.

Flow cytometry analysis of cultured cells

Following co-culture, a fraction of the generated hematopoietic progeny was harvested by vigorous pipetting from the EC layer for analysis of surface phenotype by flow cytometry (approximately 10% per well of cells cultured in bulk on AGM-EC or engineered conditions, or 50% of cells generated following single cell index culture on AGM-EC). Cells were spun and re-suspended in PBS with 2% FBS, pre-incubated with anti-mouse CD16/CD32 (FcRII block) and then stained with the following anti-mouse monoclonal antibodies: VE-Cadherin-PeCy7, CD45-PerCP, Gr-1-FITC, F4/80-FITC, Sca-1-APC, and EPCR-PE. DAPI was used to exclude dead cells. Flow cytometry was performed on a Becton Dickinson Canto 2 and data analyzed using FlowJo Software. Cells with HSC potential were identified immunophenotypically as VE-cadherin$^{-/low}$CD45$^+$Gr1$^-$F4/80$^-$Sca1^{high}EPCR^{high}. We previously showed that detection of cells with this HSC phenotype following *in vitro* culture correlated with long-term multilineage engraftment as measured by transplantation assays performed in parallel, whereas hematopoietic progeny without detectable phenotypic HSC did not provide detectable long-term multilineage hematopoietic engraftment (Hadland et al., 2017; Hadland et al., 2018).

Transplantation assays

Following co-culture, a fraction of the generated hematopoietic progeny was harvested by vigorous pipetting from the EC layer, washed with PBS with 2% FBS and re-suspended in 100 ul PBS/2% FBS per mouse transplanted. For bulk co-culture experiments on AGM-EC, the remaining 90% of cells in each well following flow cytometry analysis were pooled, washed with PBS with 2% FBS, and re-suspended at 2-3 embryo equivalent of cells per 100ul PBS/2% FBS, and combined with $5X10^4$ whole marrow cells from adult congenic C57BL/6.SJL-Ly5.1-Pep3b (CD45.1) mice in 100 ul PBS/2% FBS to provide hematopoietic rescue. For some single cell index assays, to validate the presence of functional HSCs in colonies containing hematopoietic progeny with phenotypic HSCs (VE-cadherin$^{-/low}$CD45$^+$Gr1$^-$F4/80$^-$Sca1^{high}EPCR^{high}) following co-culture, the remaining 50% volume of each 96-well was harvested for transplantation to individual mice, resuspended in 100ul, and combined with $1X10^5$ CD45.1 whole marrow cells in 100 ul PBS/2% FBS. Cell suspensions (200 ul total volume/mouse) were injected into lethally irradiated (1,000 cGy using a Cesium source) congenic CD45.1 adult recipients via the tail vein. Flow cytometry analysis of peripheral blood obtained by retro-orbital bleeds was performed at various intervals between 2 and 24 weeks following transplantation. Lineage-specific staining for donor (CD45.2) and recipient/rescue (CD45.1) cells from peripheral blood was performed as previously described (Hadland et al., 2015), using anti-mouse monoclonal antibodies indicated in the STAR Key Resources Table: CD45.1, CD45.2, CD3, CD19, Gr1, and F4/80. Multilineage engraftment was defined as $>5\%$ donor (CD45.2) contribution to the peripheral blood with contribution to each lineage of donor myeloid (Gr-1 and F4/80), B cells (CD19) and T cells (CD3) detected at $\geq 0.5\%$ at 16 to 24 weeks post-transplant, as indicated.

Quantification of HSC and HPC colony-forming cells

Following single cell index co-cultures described above, each individual sorted cell was classified based on its HSC potential. Specifically, single cells giving rise to colonies with detectable HSCs by phenotype analysis were categorized as HSC colony-forming cells (HSC-CFC); those giving rise to colonies of CD45$^+$ hematopoietic progeny lacking phenotypic HSCs were categorized as HPC colony-forming cells (HPC-CFC), and those failing to give rise to detectable hematopoietic colonies were indicated as "no colony." Results from multiple, pooled index sort experiments from E9.5-E10 (19-30 sp) were combined to quantify the total number of HSC-CFC and HPC-CFC within the VE-Cadherin$^+$CD61$^+$EPCR$^+$ (V$^+$E$^+$61$^+$) sort gate detected per P-Sp/AGM (calculated based on the number of HPC-CFC or HSC-CFC detected, the number of embryo equivalents used, and the fraction of cells in FACS that were index sorted, for each experiment) (Summarized results in Figure 1B).

Single-cell index analysis

The correlation of single cell index data with clonal hematopoietic output following co-culture was facilitated by FlowJo software (versions 9 and 10.7.1). Index sort (INX) files created at the time of index sort contained a record of florescent parameters for each sorted cell and the identity of the 96-well that it was sorted to, enabling retrospective analysis of the initial sort phenotype of clonal colonies derived from each well. FlowJo v9's 'create indexed sorting gates' function was used to create index files for each index-sorted cell,

which were subsequently classified (as HSC-CFC, HPC-CFC, etc.) based on the hematopoietic phenotype of their clonal progeny. Colony classification data was mapped onto flow plots in FlowJo v10.7.1 to evaluate the phenotypic properties of single cells as they relate to their functional output.

HPC-CFC hematopoietic lineage potential assays

Following flow cytometry analysis, a subset of hematopoietic colonies derived from index-sorted HPC-CFC were harvested for colony-forming unit (CFU) assays and OP9 co-culture to evaluate for erythroid and myeloid, and B-and T-lymphoid potential, respectively. In preparation for CFU assays, methylcellulose-based medium with recombinant cytokines was plated to 96-well tissue culture plates. The remaining HPC-CFC progeny following flow cytometry analysis were harvested by vigorous pipetting from the EC layer, washed in serum-free media, and resuspended in serum-free media. One third of the cells from each colony were added to individual 96-wells containing methylcellulose/cytokines (the remaining 2/3 were used for OP9 co-culture described below). Visual characterization of resultant CFU colonies—CFU-Erythroid (CFU-E), CFU-macrophage (CFU-M), CFU-granulocyte (GFU-G), and CFU-granulocyte/macrophage (CFU-GM) was performed under a light microscope for 10-12 days.

OP9 co-culture assay

OP9 and OP9 DLL4-expressing (OP9-DLL4) cells were plated 24-48 hours prior to OP9 co-culture initiation at a density of $1X10^4$ cells/well to gelatin-treated 24-well tissue culture plates in OP9 media. On the day of co-culture, 1mL/well of OP9 co-culture media containing FLT3L and interleukin-7 (IL-7) at 5 ng/ml each was added to OP9 24-wells in place of the OP9 media used for plating. The remaining 2/3 of HPC-CFC progeny processed as described above were divided equally and plated to OP9 or OP9-DLL4 coated wells.

After 6-7 days of co-culture, 10% of cells from the OP9 wells were harvested for flow cytometry analysis. Cells were stained in PBS with 2% FBS containing anti-mouse CD16/32 (FcRII block) and monoclonal antibodies AA4.1 (PE), B220 (Per-CP), CD19 (APC), and CD11b (APC-eFluor780). DAPI was used to exclude dead cells and contaminating GFP-expressing OP9 cells were excluded by gating on the FITC-negative population. Flow cytometry was performed on a Becton Dickinson Canto 2 and data analyzed using FlowJo Software. Isotype control-stained cells were used to set gates for analysis. B-lymphoid cells were identified phenotypically as $CD11b^-AA4.1^+CD19^+B220^+$.

After 8-11 days of co-culture (or when cells began to overgrow), 10% of cells from OP9-DLL4 co-culture were transferred to newly plated OP9-DLL4 wells. After an additional 10-13 days of culture (18-21 days total), 10% of cells from OP9-DLL4 wells were harvested for flow cytometry analysis. Cells were stained in PBS with 2% FBS containing anti-mouse CD16/32 (FcRII block) and monoclonal antibodies CD25 (PE-Cy7), CD44 (APC), CD4 (PerCP), and CD8 (PE). DAPI was used to exclude dead cells, and contaminating GFP-expressing OP9 stromal cells were excluded by gating on the FITC-negative population. Flow cytometry was performed on a Becton Dickinson Canto 2 and data analyzed using FlowJo Software. Isotype control-stained cells were used to set gates for analysis. T cells were identified phenotypically as $CD25^+CD44^-CD4^+CD8^+$.

Quantification of HPC-CFCs

Following CFU assays and OP9 co-culture as described above, the individual index-sorted HPC-CFC whose progeny were assessed in secondary assays for hematopoietic lineage potential were further classified according to their particular progenitor potentials. Specifically, HPC-CFC were sub-classified as myeloid progenitor colony-forming cells (Myeloid-CFC), erythromyeloid progenitor colony-forming cells (EMP-CFC), lymphomyeloid progenitor colony-forming cells (LMP-CFC), or multilineage progenitor colony-forming cells (MPP-CFC) according to the combination of myeloid, erythroid, and lymphoid (B cell and/or T cell) output that each HPC-CFC gave rise to in CFU and OP9 assays. Cells failing to give rise to detectable hematopoietic colonies and/or hematopoietic output in CFU/OP9 assays were indicated as "no colony/unknown." Results from multiple, pooled index sort experiments from E9-E10 (19-30 sp) were combined to quantify the total number of Myeloid-CFC, EMP-CFC, LMP-CFC, and MPP-CFC within the $VE\text{-}Cadherin^+CD61^+EPCR^+$ ($V^+E^+61^+$) sort gate detected per P-Sp/AGM (calculated based on the number of categorized progenitor colonies detected, the number of embryo equivalents used, the fraction of cells in FACS that were index sorted, and the fraction of progenitor colonies that were evaluated in secondary hematopoietic lineage assays, for each experiment) (Summarized results in Figure 2D).

Single-cell RNA sequencing

For single cell RNA sequencing (scRNA-seq) experiments, freshly sorted AGM-derived cells were washed with PBS containing 0.04% ultrapure BSA and re-suspended in 0.04% ultrapure BSA in PBS on ice. Cell suspensions were loaded into the Chromium Single Cell B Chip (10X Genomics) and processed in the Chromium single cell controller (10X Genomics), targeting a maximum of 3200 cells per lane from freshly sorted AGM-derived cells. The 10X Genomics Version 2 single cell 3′ kit was used to prepare single cell mRNA libraries with the Chromium i7 Multiplex Kit, according to manufacturer protocols. Sequencing was performed for pooled libraries from each sample on an Illumina NextSeq 500 using the 75 cycle, high output kit, targeting a minimum of 50,000 reads per cell. For AGM-derived $V^+61^+E^+$ cells, scRNA-seq was performed in two independent experiments from cells sorted from embryos pooled at E9 (27 embryos, 12-16 sp) and E9.5 (22 embryos, 15-27 sp), resulting in acquisition of 1843 individual high-quality cell sequences between E9 and E9.5. All sequencing data has been uploaded to NCBI GEO: GSE171457.

Single-cell transcriptome analysis and quality control

The Cell Ranger 2.1.1 pipeline (10X Genomics) was used to align reads to the mm10 reference genome and generate feature barcode matrix, filtering low-quality cells using default parameters. The Monocle3 (v.3.2.3.0) platform was used for downstream analysis, combining data for cells from each individual sample (as described above) for downstream analysis, using a negative binomial model of distribution with fixed variance, normalizing expression matrices by size factors. Counts for UMI (unique molecular identifiers) and unique genes expressed per cell are shown in boxplots in supplementary figures for each sample (showing median values and interquartile ranges; upper/lower whiskers show 1.5X interquartile range with outliers shown as individual dots). Cells with low UMI counts (< 5000), and cells with low genes per cell (< 1000) were removed. R scripts used for analysis are available at https://github.com/FredHutch/dignum-etal-2021.

Dimensionality reduction, batch correction, and cluster analysis

The preprocessCDS() function was used to project the data onto the top principal components (default settings), and the alignCDS() function (Haghverdi et al., 2018) was used to remove batch effects between samples using a ''mutual nearest neighbor'' algorithm, Batchelor (v.1.2.4). Uniform Manifold Approximation (UMAP) was used for dimensionality reduction with the reduceDimension() function, with reduction_method = 'UMAP'. set.seed was used to specify the number of seeds to avoid variability in output due to a random number generator in the function. Clustering was performed with the clusterCells function, with resolution = 3E-2 (Figure 3A). Given scattered expression of *Cxcr4* transcript (suggesting low level expression and gene drop-out inherent to scRNaseq data) clusters were classified as Cxcr4-positive or Cxcr4-negative based on threshold detection of *Cxcr4* transcript in > 5% of cells in each cluster (Figure 3C), resulting in classification of Cxcr4-positive cells comparable to the expected percentage of $CXCR4^+$ cells by flow cytometry (see Figure 1).

Cell type classification

Cell type classification was performed using the Garnett package (v.0.2.15) within Monocle3. Marker gene sets based on established cell type-specific genes (listed below) were used to train a classifier data (using the train_cell_classifier function with default settings) and classify cell types (using the the classify_cells function). Using this method, a small population of cells remains unclassified rather than imputing cell types for all cells in the scRNA-seq dataset. Cell type classifications were used for all downstream analyses.

Cell type	Genes expressed	Genes not expressed
Unspecified EC	*Etv2, Nr2f2*	*Runx1, Gfi1, Dll4, Ptprc*
Early arterial EC	*Dll4, Efnb2*	*Runx1, Gfi1, Etv2, Ptprc, Cd44, Gja5*
Mature arterial EC	*Cd44, Gja5*	*Runx1, Gfi1, Etv2, Ptprc*
HE	*Runx1, Gfi1*	*Etv2, Ptprc*
HPC	*Ptprc*	

Gene-set scores

Gene set scores were calculated for each single cell as the log-transformed sum of the size factor-normalized expression for each gene in published signature gene sets or from the Molecular Signatures Database (https://www.gsea-msigdb.org/gsea/msigdb/index.jsp) including: arterial EC marker genes (Aranguren et al., 2013; Luo et al., 2021; Xu et al., 2018), HSC signature genes (Cabezas-Wallscheid et al., 2017; Chambers et al., 2007; Rodriguez-Fraticelli et al., 2020; Wilson et al., 2015), HSC self-renewal genes (Asai et al., 2012; Ficara et al., 2008; Frelin et al., 2013; Jankovic et al., 2007; Jeong et al., 2009; Jude et al., 2007; Kataoka et al., 2011; Mallaney et al., 2019; Matsumoto et al., 2011; McMahon et al., 2007; Rodriguez-Fraticelli et al., 2020; Taoudi et al., 2011; Venkatraman et al., 2013; Wang et al., 2016), HE signature genes (Hou et al., 2020), AGM HSC genes (Vink et al., 2020), Dll4-regulated Myc target genes (Luo et al., 2021), hallmark Myc target genes: https://www.gsea-msigdb.org/gsea/msigdb/cards/HALLMARK_MYC_TARGETS_V1, https://www.gsea-msigdb.org/gsea/msigdb/cards/HALLMARK_MYC_TARGETS_V2, diapause signature genes (Boroviak et al., 2015; Dhimolea et al., 2021; Duy et al., 2021), senescence signature genes (Duy et al., 2021; Fridman and Tainsky, 2008) and cell cycle/proliferation genes (Srivatsan et al., 2020; Tirosh et al., 2016). Violin plots of gene-set scores based on cell types were generated using the ggplot functions geom_violin and geom_boxplot (boxplots show median values and interquartile ranges; upper/lower whiskers show 1.5X interquartile range). For statistical analysis between Cxcr4-negative HE and Cxcr4-postitive HE, Wilcoxon Rank Sum Test (ggupbr package v0.4.0) was used to calculate P values as indicated. Correlation between gene set scores are shown in scatterplots (limited to HE celltype, indicated as Cxcr4-negative HE and Cxcr4-postitive HE) generated using the ggplot functions geom_point and geom_smooth with method set to lm (linear model) to calculate a best fit regression line with 95% confidence intervals indicated by gray shadow.

Pseudotime analysis

Pseudotime trajectory analysis was performed using the learnGraph function (with prune_graph = T and ncenter = 300 settings to exclude minor trajectories that are not biologically meaningful). The order_cells function was used to calculate where each cell falls

in pseudotime. Initial pseudotime was set to cells expressing genes associated with unspecified EC as this represents the most immature cell type in the developmental hierarchy.

Gene module analysis

Gene module analysis was performed using the graph_test functions, which uses a spatial autocorrelation analysis (Moran's I) that is effective in finding genes that vary in single-cell RNA-seq datasets (Cao et al., 2019), and the find_gene_modules function to group genes into modules. For the graph_test function, neighbor_graph was set to "principle graph" to identify modules of genes that co-vary as a function of pseudotime. For the find_gene_modules, resolution was set to 4E-3. Scaled expression scores for gene modules were plotted in UMAP (Figure 3G). Moran's i and q-values (based on FDR, with FDR < 0.05 considered significant) are reported for each gene in the identified gene modules (Table S2). Gene module expression scores were plotted as a function of cluster and cell type to identify modules most specifically associated with regions of UMAP space containing Cxcr4-positive and Cxcr4-negative HE (see Figure S3H).

Differential gene expression

Differential gene expression was performed using regression analysis with the fit_models() and coefficient_table() functions in Monocle3, to identify genes that were differentially expressed based on significance values (q value) adjusted for multiple hypothesis testing using the Benjamini and Hochberg correction method. Adjusted q value < 0.05 was considered significant. Cxcr4-positive and Cxcr4-negative HE (by cell type classification) were compared for this analysis, to identify differentially expressed genes in the whole genome (genome-wide, limited to genes expressed in at least 10 cells in the cell dataset) (full gene list provided in Table S4). AGM HSC signature genes (Vink et al., 2020) and compiled adult HSC signature genes from published datasets (Cabezas-Wallscheid et al., 2017; Chambers et al., 2007; Rodriguez-Fraticelli et al., 2020; Wilson et al., 2015) were used identify the subset of genes in Cxcr4-positive versus Cxcr4-negative HE that overlap with HSC signature genes (Figures S4C and S4D).

Gene Ontology (GO) analysis

Gene enrichment analysis was performed using two online functional annotations tools, DAVID v6.8 (Huang et al., 2009a, 2009b) or AmiGO v2.5.13 (Ashburner et al., 2000; Carbon et al., 2009; Gene Ontology Consortium, 2021). Lists of gene short names for genes found to be significantly upregulated in Cxcr4-postive or Cxcr4-negative HE were uploaded and mapped to database gene IDs. Functional annotation clustering was performed to identify overrepresented GO-terms for biological processes. Specifically, the 'GO-FAT' and 'GO biological process complete' algorithms were used for analysis with DAVID and AmiGO, respectively. The top 10 GO-terms from each analysis, as defined by Bonferroni corrected p values, are reported graphically (Figures S4A and S4B), while the full analysis can be found in Table S4.

QUANTIFICATION AND STATISTICAL ANALYSIS

Statistical analyses of colony frequencies were conducted with Prism. Data are expressed as mean ± standard error (s.e.m), and *n* indicates biological repeats, unless indicated otherwise. P values calculated by Student's t test unless otherwise indicated.